buildings

MDPI

Article

Sound Absorption Characteristics of Unsaturated Porous Material Calculated by Modified Transfer Matrix Method

Yiguo Yin [1,2] and Wei Guan [1,*]

[1] Department of Astronautics and Mechanics, Harbin Institute of Technology, Harbin 150001, China; yinyiguo3256@sina.com
[2] Beijing Institute of Astronautical Systems Engineering, Beijing 100000, China
* Correspondence: guanw@hit.edu.cn

Abstract: Porous materials have emerged as one of the most widely employed sound-absorbing materials in practical applications, owing to their excellent sound absorption properties and lightweight nature. Unsaturated porous materials have the potential to achieve superior sound absorption effects and significantly reduce mass. However, current research on the sound absorption performance of unsaturated porous materials is limited. This paper used a modified transfer matrix method (MTMM), which relies on matrix dimensionality reduction, to analyze the sound absorption characteristics of unsaturated porous materials under various boundary conditions. The study also examines the impact of different parameters, such as material thickness and saturation, on sound absorption performance and compares the results. The findings indicate that when a solid elastic plate is attached to an unsaturated porous elastic plate, the absorption coefficient decreases while the transmission loss increases. Additionally, reducing the thickness of the plate and increasing its porosity and saturation levels lead to an increase in the absorption coefficient and a decrease in the transmission loss.

Keywords: sound absorption characteristics; unsaturated porous material; modified transfer matrix method; saturation

check for updates

Citation: Yin, Y.; Guan, W. Sound Absorption Characteristics of Unsaturated Porous Material Calculated by Modified Transfer Matrix Method. *Buildings* **2024**, *14*, 466. https://doi.org/10.3390/buildings14020466

Academic Editors: Angela D. La Rosa and Antonio Caggiano

Received: 12 December 2023
Revised: 25 January 2024
Accepted: 5 February 2024
Published: 7 February 2024

Copyright: © 2024 by the authors. Licensee MDPI, Basel, Switzerland. This article is an open access article distributed under the terms and conditions of the Creative Commons Attribution (CC BY) license (https://creativecommons.org/licenses/by/4.0/).

1. Introduction

In recent years, the use of porous materials in construction has witnessed a gradual rise, extending to applications in walls, roofs, interior decoration, and other building materials. In comparison to conventional materials, these materials offer distinct advantages, including a porous microstructure, lower mass density, efficient heat transfer, moisture absorption capabilities, and notable sound absorption performance. These features collectively contribute to the creation of a more comfortable living environment, aligning with and addressing various human living needs. Numerous studies have delved into the efficacy of porous materials as building components. Santos and Mendes [1], for instance, devised a mathematical model for unsaturated sandy roofs, aiming to predict the influence of such roofs on the passive cooling of buildings. Bennai et al. [2] explored a macroscopic convective fluid heat transfer model employing unsaturated porous materials as heat sources that helped seek a deeper understanding of building material behavior and enhance predictions of energy performance. Liu [3], Chen [4], and other researchers directed their attention toward the evaporation and condensation performance of unsaturated porous building materials. This focus holds particular significance for passive indoor heating and the passive evaporation dynamics of porous walls. Scholarly investigations into the combined transfer of heat, gas, and water in porous materials represent a pivotal area of research as well [5]. Nevertheless, with the development of urban architecture, various noises have greatly affected the living experience and quality of life of urban residents. Consequently, global scholars have increasingly focused on noise control research. The adoption of sound-absorbing materials has emerged as a proven and effective strategy for

mitigating noise, with porous materials standing out as the preferred choice due to their remarkable sound-absorbing capabilities and lightweight attributes.

The sound absorption mechanism of porous materials is attributed to their numerous interconnected micropores, which enable sound waves to penetrate the material and dissipate sound energy through heat loss resulting from friction between air molecules and pore walls, as well as viscous losses within the airflow inside the material [6]. Based on this principle, there have been many studies aimed at further enhancing the sound absorption performance of porous materials. Ning and Zhao [7] suggested a structure of multilayer porous metal material with an air-backed layer to improve the sound absorption performance under positive incidence. The results indicated that the sound absorption performance of multilayer porous metal material was superior to that of single-layer porous material when the air-backed layer was of the same thickness. Zhu et al. [8] studied the sound absorption performance of gradient porous materials made by covering and sintering multiple layers of stainless steel fibers with different diameters, demonstrating that gradient porous structures can notably enhance sound absorption performance. Gao et al. [9] proposed a composite material with ribs embedded in porous materials, which achieved an average absorption coefficient of 0.937 in the frequency range of less than 10 kHz. This demonstrated the superior sound absorption capabilities of the composite material. Afterwards, they [10] developed a composite porous metamaterial with multiple layers of I-shaped plates, which can effectively absorb and dissipate sound energy at different frequencies. Moreover, Choy, Huang, and Wang [11] investigated the possibility of filling porous materials with low-density gas to extend the effective frequency range of sound absorption to lower frequencies and conducted experimental confirmation to support their findings. The research on the sound transmission loss of a two-plate functionally graded sandwich structure with a porous core has demonstrated that the use of FGP plates and absorbers can increase sound transmission loss, and the simultaneous use of both is effective at high frequencies [12]. W.H. Yuan et al. [13] have also carried out similar work, and their research object is a porous foam functional gradient plate under the influence of a temperature field.

The infusion of gas into liquid-saturated porous materials induces noteworthy alterations in the diverse mechanical properties of these materials. As early as 1974, Domenico [14] studied the effect of water saturation on the material properties of an unsaturated material (mud shale sandstone reservoir) and found that the characteristics of the material varied with water saturation. Tuncay and Corapcioglu [15] presented a theory of wave propagation in poroelastic media that are saturated with two mutually incompatible Newtonian fluids and studied the wave propagation properties of this material. The study by Lo et al. [16] revealed a correlation between the attenuation of elastic waves in porous materials saturated with both gas and water phases, variations in material density, and the relative mobility of the pore fluids. Based on Biot theory [17–19], Garg et al. [20] and Kang et al. [21] developed internal intrinsic constitutive relationships for gas–liquid saturated porous materials. Berryman et al. [22] calculated the propagation properties of bulk elastic waves in partially saturated porous solids, including propagation velocity and attenuation. However, there has been limited research on the sound absorption capabilities of unsaturated porous materials.

Due to its high computational efficiency, accurate calculation results, and no need to establish the global dynamic equations of the system, the transfer matrix method has been one of the most widely used methods for calculating the sound absorption properties of porous materials. Yun et al. [23] developed a generalized solution for finite-amplitude nonlinear acoustic waves in a laminar system using the second-order transfer matrix approach to compute the propagation of such waves in a periodic laminar system. Lin et al. [24,25] employed the transfer matrix method to establish a model for the propagation of acoustic waves in composites with diverse boundary conditions and assessed the acoustic transmission loss in an orthotropic anisotropic composite material. Shahsavari et al. [26] used the transfer matrix method to determine the local transfer matrix of each sublayer in a functionally graded porous cylindrical shell, and their product created the global transfer

matrix of the structure, which enabled the computation of acoustic wave propagation in the cylindrical shell. The traditional transfer matrix method has some drawbacks, such as complex matrix elements and inflexibility in adapting to changes in boundary conditions. As a result, many scholars have made effective modifications to this method to address these issues. Castaings and Hosten [27] presented and validated an improved transfer matrix method for calculating the propagation of nonuniform plane waves in submerged multilayers made of anisotropic absorption layers. X.Z. Zhang et al. [28] conducted a simplified static analysis of the transfer matrix for multi-body systems, expanding the application scope of the transfer matrix method for multi-body systems. H.J. Lu et al. [29] proposed a new transfer matrix method for vibration analysis of flexible multibody systems, which has the advantages of easy derivation of the overall transfer equation, low system matrix order, and fast calculation speed. Khurana et al. [30] simplified the matrix element expressions in the transfer matrix method, and Parrinello et al. [31] developed a precise and efficient generalized transfer matrix method for planar structures with periodic features in the plane. Xue [32] modified the transfer matrix method by reducing matrix dimensionality, which facilitates flexible coupling and modification of multilayer structure modeling even though the number of propagation waves in the layers increases.

Although many scholars have conducted sufficient research on the sound absorption performance of porous materials, there is still relatively little research on unsaturated porous materials in this area, and using gas instead of some pore fluids can effectively reduce the weight of materials, which is very beneficial in the field of construction. The application of the modified transfer matrix method to complex structures of this type of material can make calculations more convenient and efficient. This study employs the modified transfer matrix method (MTMM) proposed by Xue [32] to model the propagation of acoustic waves in unsaturated porous materials under various conditions, including those with air exposure, elastic plates adhered to the top/bottom end, and elastic plates adhered to both the top and bottom ends. The absorption coefficients and transmission losses of these structures are calculated accordingly. Furthermore, the impacts of varying material parameters on the absorption coefficient and transmission loss were examined, which include the thickness of the porous plate, porosity, saturation, and the angle of the incident wave.

2. Modeling of Unsaturated Porous Media

In this section, we examine porous media where the pores are filled with both liquids and gases, resulting in three phases in the material: the solid matrix, the gas phase, and the liquid phase. Assume that the volume fractions of the solid phase, liquid phase, and gas phase occupying the material are ϕ_s, ϕ_l, and ϕ_g respectively, where $\phi = \phi_l + \phi_g$ is porosity and $\phi_s = 1 - \phi$. For convenience, the symbols used in the article are summarized into a symbol list, which is provided in Appendix A. Moreover, the concept of relative saturation for the gas and liquid phases was introduced based on Biot theory. Here, $S_l = \phi_l/\phi$ denotes the relative saturation of the liquid phase, while $S_g = \phi_g/\phi$ denotes the relative saturation of the gas phase. Consequently, the total stress in the unsaturated porous material can be separated into contributions from the solid, liquid, and gas phases [21]:

$$\tau = \tau^s + \tau^l + \tau^g, \tag{1}$$

where the superscripts s, l, and g represent the solid phase, liquid phase, and gas phase, respectively. The constitutive relations for the unsaturated porous medium can be expressed as follows:

$$\begin{aligned} \tau_{ij}^s &= 2\mu\varepsilon_{ij}^s + \left[\left(a_{11} - \tfrac{2}{3}\mu\right)\varepsilon_{kk}^s + a_{12}\varepsilon_{kk}^g + a_{13}\varepsilon_{kk}^l\right]\delta_{ij}, \\ \tau_{ij}^g &= \left(a_{21}\varepsilon_{kk}^s + a_{22}\varepsilon_{kk}^g + a_{23}\varepsilon_{kk}^l\right)\delta_{ij},\ \tau_{ij}^l = \left(a_{31}\varepsilon_{kk}^s + a_{32}\varepsilon_{kk}^g + a_{33}\varepsilon_{kk}^l\right)\delta_{ij}, \end{aligned} \tag{2}$$

where $\varepsilon_{ij}^{s} = \frac{1}{2}\left(u_{i,j}^{s} + u_{j,i}^{s}\right)$ represents the strain tensor of the solid frame; u is the displacement; and $\varepsilon_{kk}^{n} = \nabla \cdot u^{n} (n = s, l, g)$ denotes the body strains of the solid, fluid, and gas phases, respectively. The parameter μ denotes the shear modulus of the solid frame. The other parameters in Equation (2) are material constants that can be calculated using the following expressions:

$$\begin{array}{l} a_{11} = K_b, \quad a_{12} = a_{21} = K_g\phi_s S_g(A_1 + K_l)/D, \quad a_{13} = a_{31} = K_l\phi_s S_l\left(A_1 + K_g\right)/D, \\ a_{22} = K_g\phi_g\left(S_g K_l + A_1\right)/D, \; a_{23} = a_{32} = K_g K_l S_g S_l\phi/D, \; a_{33} = K_l\phi_l\left(S_l K_g + A_1\right)/D, \\ D = K_g S_l + A_1 + K_l S_g, \quad A_1 = S_g S_l \cdot dP_c/dS_g, \quad P_c = \alpha_{vg}^{-1}\left(S_l^{\,-m_{vg}^{-1}} - 1\right)^{1-m_{vg}}, \end{array} \tag{3}$$

where K_b, K_l, and K_g are the bulk moduli of the drained porous frame, gas phase, and liquid phase, respectively. P_c is a function describing the capillary pressure, ignoring the hysteresis effect. α_{vg} and m_{vg} are the van Genuchten model parameters [33].

Following the assumption of infinitesimal deformation and neglecting the body forces, the kinetic equation of the unsaturated porous material can be written as:

$$\begin{array}{l} \rho_s\phi_s\ddot{u}_s = \tau_{ji,j}^{s} + d_g\left(\dot{u}_g - \dot{u}_s\right) + d_l\left(\dot{u}_l - \dot{u}_s\right), \\ \rho_l\phi_l\ddot{u}_l = \tau_{ji,j}^{l} - d_l\left(\dot{u}_l - \dot{u}_s\right), \; \rho_g\phi_g\ddot{u}_g = \tau_{ji,j}^{g} - d_g\left(\dot{u}_g - \dot{u}_s\right), \end{array} \tag{4}$$

where $\rho_n (n = s, l, g)$ denote the densities of the solid phase, liquid phase, and gas phase, respectively, and d_l and d_g are coefficients related to viscous drag, and they are expressed as follows:

$$d_g = \frac{\phi_g^2\eta_g}{\kappa_s\kappa_{rg}}, \quad d_l = \frac{\phi_l^2\eta_l}{\kappa_s\kappa_{rl}}, \tag{5}$$

where $\kappa_{rg} = \sqrt{1 - S_l}\left(1 - S_l^{\frac{1}{m}}\right)^{2m}$ and $\kappa_{rl} = \sqrt{S_l}\left[1 - \left(1 - S_l^{\frac{1}{m}}\right)^{m}\right]^2$ are the relative permeabilities of the gas phase and liquid phase, respectively, and κ_s is the absolute permeability of the unsaturated porous material. η_l and η_g are the dynamic shear viscosities of the liquid and gas phases, respectively.

By substituting the constitutive relations from Equation (2) into Equation (4), the motion equations for unsaturated porous materials based on displacements can be derived as follows:

$$\begin{array}{l} \rho_s\phi_s\ddot{u}_s - d_g\left(\dot{u}_g - \dot{u}_s\right) - d_l\left(\dot{u}_l - \dot{u}_s\right) = \nabla\left[\left(a_{11} + \frac{\mu}{3}\right)\nabla\cdot u_s + a_{12}\nabla\cdot u_g + a_{13}\nabla\cdot u_l\right] + \mu\nabla^2 u_s, \\ \rho_g\phi_g\ddot{u}_g + d_g\left(\dot{u}_g - \dot{u}_s\right) = \nabla\left(a_{21}\nabla\cdot u_s + a_{22}\nabla\cdot u_g + a_{23}\nabla\cdot u_l\right), \\ \rho_l\phi_l\ddot{u}_l + d_l\left(\dot{u}_l - \dot{u}_s\right) = \nabla\left(a_{31}\nabla\cdot u_s + a_{32}\nabla\cdot u_g + a_{33}\nabla\cdot u_l\right). \end{array} \tag{6}$$

To solve Equation (6), the Helmholtz decomposition is applied to the following three displacement vectors:

$$u_s = \nabla\psi_s + \nabla\times H_s, \; u_g = \nabla\psi_g + \nabla\times H_g, \; u_l = \nabla\psi_l + \nabla\times H_l, \tag{7}$$

where $\psi_n (n = s, l, g)$ and $H_n (n = s, l, g)$ are the potential functions of P and S waves, respectively. By substituting the expressions in Equation (7) into the motion equations of Equation (6), we can obtain the following:

$$\begin{array}{c} \rho_s\phi_s\left(\nabla\ddot{\psi}_s + \nabla\times\ddot{H}_s\right) - d_g\left(\nabla\dot{\psi}_g + \nabla\times\dot{H}_g - \nabla\dot{\psi}_s + \nabla\times\dot{H}_s\right) \\ -d_l\left(\nabla\dot{\psi}_l + \nabla\times\dot{H}_l - \nabla\dot{\psi}_s + \nabla\times\dot{H}_s\right) = \nabla\left[\left(a_{11} + \frac{\mu}{3}\right)\nabla\cdot(\nabla\psi_s + \nabla\times H_s)\right. \\ \left.+a_{12}\nabla\cdot\left(\nabla\psi_g + \nabla\times H_g\right) + a_{13}\nabla\cdot(\nabla\psi_l + \nabla\times H_l)\right] + \mu\nabla^2(\nabla\psi_s + \nabla\times H_s), \\ \rho_g\phi_g\left(\nabla\ddot{\psi}_g + \nabla\times\ddot{H}_g\right) + d_g\left(\nabla\dot{\psi}_g + \nabla\times\dot{H}_g - \nabla\dot{\psi}_s - \nabla\times\dot{H}_s\right) = \\ \nabla\left[a_{21}\nabla\cdot(\nabla\psi_s + \nabla\times H_s) + a_{22}\nabla\cdot\left(\nabla\psi_g + \nabla\times H_g\right) + a_{23}\nabla\cdot(\nabla\psi_l + \nabla\times H_l)\right], \\ \rho_l\phi_l\left(\nabla\ddot{\psi}_l + \nabla\times\ddot{H}_l\right) + d_l\left(\nabla\dot{\psi}_l + \nabla\times\dot{H}_l - \nabla\dot{\psi}_s - \nabla\times\dot{H}_s\right) = \\ \nabla[a_{31}\nabla\cdot(\nabla\psi_l + \nabla\times H_l) + a_{32}\nabla\cdot(\nabla\psi_l + \nabla\times H_l) + a_{33}\nabla\cdot(\nabla\psi_l + \nabla\times H_l)]. \end{array} \tag{8}$$

The above equation was simplified, and the divergence operation was applied to obtain the equation that the P wave should satisfy:

$$\begin{aligned}\rho_s\phi_s\ddot{\psi}_s - d_g\left(\dot{\psi}_g - \dot{\psi}_s\right) - d_l\left(\dot{\psi}_l - \dot{\psi}_s\right) &= \left(a_{11} + \tfrac{4\mu}{3}\right)\nabla^2\psi_s + a_{12}\nabla^2\psi_g + a_{13}\nabla^2\psi_l,\\ \rho_g\phi_g\ddot{\psi}_g + d_g\left(\dot{\psi}_g - \dot{\psi}_s\right) &= a_{21}\nabla^2\psi_s + a_{22}\nabla^2\psi_g + a_{23}\nabla^2\psi_l,\\ \rho_l\phi_l\ddot{\psi}_l + d_l\left(\dot{\psi}_l - \dot{\psi}_s\right) &= a_{31}\nabla^2\psi_s + a_{32}\nabla^2\psi_g + a_{33}\nabla^2\psi_l,\end{aligned} \tag{9}$$

where the time term is assumed to be $e^{-i\omega t}$, so $\ddot{\psi} = -\omega^2\psi$ and $\dot{\psi} = -i\omega\psi$. The potential functions for the displacements of the fluid phase and gas phase relative to the solid skeleton are assumed to have the same form as those for the solid skeleton. The relevant coefficients A_l and A_g for P waves are multiplied by the potential functions. The characteristic equation satisfied by the P wave can be obtained by substituting these relations into Equation (9) and organizing it as follows:

$$\begin{bmatrix} H_1k_p^2 - \omega^2\rho_s\phi_s - i\omega\left(d_g + d_l\right) & a_{12}k_p^2 + i\omega d_g & a_{13}k_p^2 + i\omega d_l \\ a_{21}k_p^2 + i\omega d_g & a_{22}k_p^2 - \omega^2\rho_g\phi_g - i\omega d_g & a_{23}k_p^2 \\ a_{31}k_p^2 + i\omega d_l & a_{32}k_p^2 & a_{33}k_p^2 - \omega^2\rho_l\phi_l - i\omega d_l \end{bmatrix}\begin{bmatrix} 1 \\ A_g \\ A_l \end{bmatrix} = \begin{bmatrix} 0 \\ 0 \\ 0 \end{bmatrix}. \tag{10}$$

where $H_1 = a_{11} + 4\mu/3$. The wave numbers of P waves in unsaturated porous materials can be determined by solving Equation (10), which in turn yields the propagation velocities. It can be observed that there are three distinct P waves present in unsaturated porous materials. We can perform the curl operation on Equation (8), followed by the relevant simplification steps, to obtain the corresponding characteristic equation for the S wave as follows:

$$\begin{bmatrix} \mu k_s^2 - \omega^2\rho_s\phi_s - i\omega\left(d_g + d_l\right) & i\omega d_g & i\omega d_l \\ i\omega d_g & -\omega^2\rho_g\phi_g - i\omega d_g & 0 \\ i\omega d_l & 0 & -\omega^2\rho_l\phi_l - i\omega d_l \end{bmatrix}\begin{bmatrix} 1 \\ B_g \\ B_l \end{bmatrix} = \begin{bmatrix} 0 \\ 0 \\ 0 \end{bmatrix}, \tag{11}$$

where B_g and B_l are the relative coefficients for S waves between the gas phase, fluid phase, and solid frame, respectively. According to Equation (11), there is only one S wave present in unsaturated porous materials.

By solving the above two equations separately, the expressions for the wave numbers (pf) of P waves and S waves in unsaturated porous materials can be obtained, and based on this, the structure in the next section can be modeled.

3. Modified Transfer Matrix Method

Figure 1 depicts an unsaturated porous elastic plate of thickness d exposed to air, with z = 0 denoting its lowest surface. Acoustic waves are incident on the lower surface with an incidence angle of θ. In order to provide a simple and convenient explanation of the application of the modified transfer matrix method in the propagation of elastic waves in unsaturated porous materials and to compare it with the bonding situation between porous materials and rigid panels, we use the situation in Figure 1 to derive and explain the modified transfer matrix method, laying a foundation for its bonding with the elastic layer. To calculate the sound absorption properties of a structure that involves an unsaturated porous elastic plate, we use the sound pressure p and sound velocity v_z in the air as state vectors. These state vectors on both sides of the plate are connected through a total transfer matrix $[T]$, expressed in Equation (12), which we need to determine to calculate the sound absorption properties of the structure.

$$[p \;\; v_z]_{z=0}^{\mathrm{T}} = [T]_{2\times2}[p \;\; v_z]_{z=d}^{\mathrm{T}}, \tag{12}$$

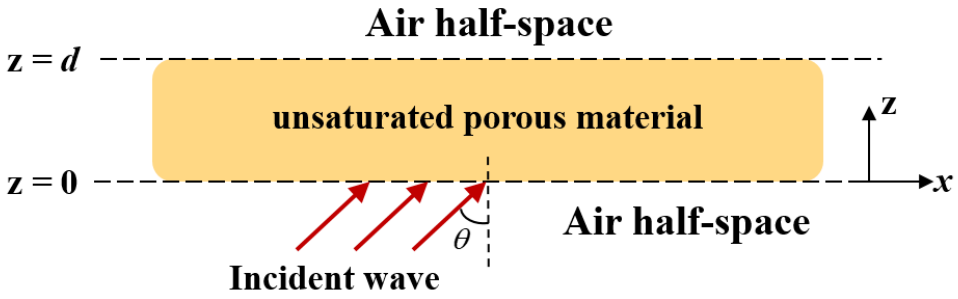


Figure 1. Sound wave incident into an unsaturated porous elastic plate exposed to air.

The boundary conditions on the upper and lower surfaces of the unsaturated porous elastic plate can be expressed in this case as:

$$\begin{array}{c} \tau_z^s = -(1-\phi_g-\phi_l)p,\ \tau_z^g = -\phi_g p,\ \ \tau_z^l = -\phi_l p, \\ i\omega\phi_s u_z^s + i\omega\phi_g u_z^g + i\omega\phi_l u_z^l = v_z, \qquad \tau_{xz} = 0, \end{array} \tag{13}$$

where $\tau_z^n (n = s, l, g)$ is the normal stress in the solid, liquid, and gas phases in the unsaturated porous elastic plate; τ_{xz} is the tangential stress of the elastic plate; $u_z^n (n = s, l, g)$ is the normal displacement of each phase; i is an imaginary unit; and ω is the frequency. The boundary conditions can be expressed in the following matrix form:

Lower surface:

$$[M_1]_{5\times 8}\begin{bmatrix}\tau_z^s & u_z^s & \tau_z^g & u_z^g & \tau_z^l & u_z^l & \tau_{xz}^s & u_x^s\end{bmatrix}_{z=0}^{\mathrm{T}} = [N_1]_{5\times 2}\begin{bmatrix}p & v_z\end{bmatrix}_{z=0}^{\mathrm{T}}, \tag{14}$$

Upper surface:

$$[M_2]_{5\times 8}\begin{bmatrix}\tau_z^s & u_z^s & \tau_z^g & u_z^g & \tau_z^l & u_z^l & \tau_{xz}^s & u_x^s\end{bmatrix}_{z=d}^{\mathrm{T}} = [N_2]_{5\times 2}\begin{bmatrix}p & v_z\end{bmatrix}_{z=d}^{\mathrm{T}}, \tag{15}$$

The matrices $[M]$ and $[N]$ can be obtained as:

$$[M_1]_{5\times 8} = [M_2]_{5\times 8} = \begin{bmatrix} 1 & 0 & 0 & 0 & 0 & 0 & 0 & 0 \\ 0 & 0 & 1 & 0 & 0 & 0 & 0 & 0 \\ 0 & 0 & 0 & 0 & 1 & 0 & 0 & 0 \\ 0 & i\omega\phi_s & 0 & i\omega\phi_g & 0 & i\omega\phi_l & 0 & 0 \\ 0 & 0 & 0 & 0 & 0 & 0 & 1 & 0 \end{bmatrix}, \tag{16}$$

$$[N_1]_{5\times 2} = [N_2]_{5\times 2} = \begin{bmatrix} -\phi_s & 0 \\ -\phi_g & 0 \\ -\phi_l & 0 \\ 0 & 1 \\ 0 & 0 \end{bmatrix}, \tag{17}$$

The vectors of stresses and displacements at the upper and lower surfaces of the unsaturated porous elastic plate can be connected by the internal transfer matrix $[T_i]$ of the plate:

$$\begin{array}{c} \begin{bmatrix}\tau_z^s & u_z^s & \tau_z^g & u_z^g & \tau_z^l & u_z^l & \tau_{xz}^s & u_x^s\end{bmatrix}_{z=0}^{\mathrm{T}} = \\ [T_i]_{8\times 8}\begin{bmatrix}\tau_z^s & u_z^s & \tau_z^g & u_z^g & \tau_z^l & u_z^l & \tau_{xz}^s & u_x^s\end{bmatrix}_{z=d}^{\mathrm{T}} \end{array}, \tag{18}$$

where the matrix $[T_i]$ can be calculated by $[T_i] = [C]_{z=0}[C]_{z=d}^{-1}$, and the elements of $[C]$ are listed in Appendix B. To obtain the form of $[T_i]$ as presented in Equation (12), the MTMM proposed by Xue [28] involves a series of treatments for Equations (14)–(18). The first

step involves performing the singular value decomposition (SVD) of the matrix $[N_1]$, as presented in Equation (14):

$$[N_1]_{5\times2} = [U_1]_{5\times5}[S_1]_{5\times2}[V_1]^{\mathrm{H}}_{2\times2}, \tag{19}$$

The superscript H represents the conjugate transpose of the matrix. Then, Equation (14) can be rewritten in the following form:

$$[M_1]_{5\times8}\begin{bmatrix}\tau_z^s & u_z^s & \tau_z^g & u_z^g & \tau_z^l & u_z^l & \tau_{xz}^s & u_x^s\end{bmatrix}^{\mathrm{T}}_{z=0} = [U_1]_{5\times5}[S_1]_{5\times2}[V_1]^{\mathrm{H}}_{2\times2}\begin{bmatrix}p & v_z\end{bmatrix}^{\mathrm{T}}_{z=0}, \tag{20}$$

where $[S_1]_{5\times2} = \begin{bmatrix}[S_{1a}]_{2\times2}\\ [0]_{3\times2}\end{bmatrix}$, and $[S_{1a}]_{2\times2} = \begin{bmatrix}\lambda_1 & 0\\ 0 & \lambda_2\end{bmatrix}$ with λ_1 and λ_2 are the singular values of the matrix $[N_1]$. Next, the matrix $[A]$ is divided into upper and lower parts: $[A]_{5\times8} = \begin{vmatrix}[Aa]_{2\times8}\\ [Ab]_{3\times8}\end{vmatrix} = [U_1]^{\mathrm{H}}_{5\times5}[M_1]_{5\times8}$, corresponding to the matrix $[S_1]$.

In this way, Equation (20) can also be divided into upper and lower parts:

$$\begin{bmatrix}[Aa]_{2\times8}\\ [Ab]_{3\times8}\end{bmatrix}\begin{bmatrix}\tau_z^s & u_z^s & \tau_z^g & u_z^g & \tau_z^l & u_z^l & \tau_{xz}^s & u_x^s\end{bmatrix}^T_{z=0} = \begin{bmatrix}\lambda_1 & 0\\ 0 & \lambda_2\\ \hline [0]_{3\times2}\end{bmatrix}[V_1]^{\mathrm{H}}_{2\times2}\begin{bmatrix}p\\ v_z\end{bmatrix}_{z=0}. \tag{21}$$

If we disregard the lower part of Equation (21) and multiply matrices $[S_{1a}]^{-1}$ and $[V_1]_{2\times2}$ in the upper part, the following equation can be obtained:

$$[V_1]_{2\times2}[S_{1a}]^{-1}_{2\times2}[Aa]_{2\times8}\begin{bmatrix}\tau_z^s & u_z^s & \tau_z^g & u_z^g & \tau_z^l & u_z^l & \tau_{xz}^s & u_x^s\end{bmatrix}^{\mathrm{T}}_{z=0} = \begin{bmatrix}p & v_z\end{bmatrix}^{\mathrm{T}}_{z=0}, \tag{22}$$

Here, we define a coupling matrix $[C_1]_{5\times8} = \begin{bmatrix}[C_{1a}]_{2\times8} & [C_{1b}]_{3\times8}\end{bmatrix}^{\mathrm{T}}$, such that it satisfies the equation:

$$[C_1]_{5\times8}\begin{bmatrix}\tau_z^s & u_z^s & \tau_z^g & u_z^g & \tau_z^l & u_z^l & \tau_{xz}^s & u_x^s\end{bmatrix}^{\mathrm{T}}_{z=0} = \begin{bmatrix}p & v_z & 0 & 0 & 0\end{bmatrix}^{\mathrm{T}}_{z=0}. \tag{23}$$

The submatrix can be expressed as $[C_{1a}]_{2\times8} = [V_1]_{2\times2}[S_{1a}]^{-1}_{2\times2}[Aa]_{2\times8}$, $[C_{1b}]_{3\times8} = [Ab]_{3\times8}$.

Next, we need to address the boundary conditions of the upper layer of the elastic plate so that the state vector in the air on the upper side has the same matrix dimension as that in Equation (23). To achieve this, we perform the following SVD on the matrix $[M_2]$ in Equation (15):

$$[M_2]_{5\times8} = [U_2]_{5\times5}[S_2]_{5\times8}[V_2]^{\mathrm{H}}_{8\times8},\ [S_2]_{5\times8} = \begin{bmatrix}[\Sigma]_{5\times5} & [0]_{5\times3}\end{bmatrix}. \tag{24}$$

Therefore, Equation (15) is written in the following form:

$$\begin{bmatrix}[\Sigma]_{5\times5}\big|[0]_{5\times3}\end{bmatrix}[V_2]^{\mathrm{H}}_{8\times8}\begin{bmatrix}\tau_z^s & u_z^s & \tau_z^g & u_z^g & \tau_z^l & u_z^l & \tau_{xz}^s & u_x^s\end{bmatrix}^{\mathrm{T}}_{z=d} = [B]^{\mathrm{H}}_{5\times2}\begin{bmatrix}p & v_z\end{bmatrix}^{\mathrm{T}}_{z=d}, \tag{25}$$

in which $[B]_{5\times2} = [U_2]^{\mathrm{H}}_{5\times5}[N_2]_{5\times2}$.

Unlike the lower boundary processing, which involves dividing the matrix $[S_1]$ into two pieces, the upper boundary processing requires adding elements to the matrix $[S_2]$ to make it a square matrix. Correspondingly, the matrix $[B]^{\mathrm{H}}$ and the state vector in the upper air need to be supplemented. Then, the following equation can be obtained:

$$\begin{bmatrix}[\Sigma]_{5\times5} & [0]_{5\times3}\\ [0]_{3\times5} & [\mathrm{I}]_{3\times3}\end{bmatrix}[V_2]^{\mathrm{H}}_{8\times8}\begin{bmatrix}\tau_z^s & u_z^s & \tau_z^g & u_z^g & \tau_z^l & u_z^l & \tau_{xz}^s & u_x^s\end{bmatrix}^{\mathrm{T}}_{z=d} = \begin{bmatrix}[B]_{5\times2} & [0]_{5\times3}\\ [0]_{3\times2} & [\mathrm{I}]_{3\times3}\end{bmatrix}\begin{bmatrix}p & v_z & X_1 & X_2 & X_3\end{bmatrix}^{\mathrm{T}}_{z=d}, \tag{26}$$

Keeping only the state vector at the left end of Equation (26), the above equation can be written as follows:

$$\begin{bmatrix} \tau_z^s & u_z^s & \tau_z^g & u_z^g & \tau_z^l & u_z^l & \tau_{xz}^s & u_x^s \end{bmatrix}_{z=d}^{\mathrm{T}} = [V_2]_{8\times8}\begin{bmatrix} [S]_{5\times5}^{-1} & [0]_{5\times3} \\ [0]_{3\times5} & [I]_{3\times3} \end{bmatrix}\begin{bmatrix} [B]_{5\times2} & [0]_{5\times3} \\ [0]_{3\times2} & [I]_{3\times3} \end{bmatrix}\begin{bmatrix} p & v_z & X_1 & X_2 & X_3 \end{bmatrix}_{z=d}^{\mathrm{T}}, \tag{27}$$

Let the coupling matrix $[C_2]_{8\times5} = [V_2]_{8\times8}\begin{bmatrix} [\Sigma]_{5\times5}^{-1} & [0]_{5\times3} \\ [0]_{3\times5} & [\mathrm{I}]_{3\times3} \end{bmatrix}\begin{bmatrix} [B]_{5\times2} & [0]_{5\times3} \\ [0]_{3\times2} & [\mathrm{I}]_{3\times3} \end{bmatrix}$, then Equation (27) has the same form as Equation (23), which is what we desired:

$$\begin{bmatrix} \tau_z^s & u_z^s & \tau_z^g & u_z^g & \tau_z^l & u_z^l & \tau_{xz}^s & u_x^s \end{bmatrix}_{z=d}^{\mathrm{T}} = [C_2]_{8\times5}\begin{bmatrix} p & v_z & X_1 & X_2 & X_3 \end{bmatrix}_{z=d}^{\mathrm{T}}, \tag{28}$$

By combining Equations (18), (23), and (28), the relationship between the state vectors in air after dimensionality increase can be obtained as follows:

$$\begin{bmatrix} p & v_z & 0 & 0 & 0 \end{bmatrix}_{z=0}^{\mathrm{T}} = [C_1]_{5\times8}[T]_{8\times8}[C_2]_{8\times5}\begin{bmatrix} p & v_z & X_1 & X_2 & X_3 \end{bmatrix}_{z=d}^{\mathrm{T}}. \tag{29}$$

From Equation (29), we conclude a dimension-reduced transfer matrix $[T_{SVD}]_{5\times5} = [C_1]_{5\times8}[T]_{8\times8}[C_2]_{8\times5}$, and then we perform QR decomposition on it:

$$\begin{bmatrix} p & v_z & 0 & 0 & 0 \end{bmatrix}_{z=0}^{\mathrm{T}} = [Q]_{5\times5}[R]_{5\times5}\begin{bmatrix} p & v_z & X_1 & X_2 & X_3 \end{bmatrix}_{z=d}^{\mathrm{T}}. \tag{30}$$

The two ends of Equation (30) are multiplied by the matrix $[Q]_{5\times5}^{\mathrm{H}}$:

$$[Q]_{5\times5}^{\mathrm{H}}\left|\begin{matrix} 1 & 0 \\ 0 & 1 \\ \hline [0] & \end{matrix}\right|\begin{bmatrix} p \\ v_z \end{bmatrix}_{z=0} = [R]_{5\times5}\begin{bmatrix} p & v_z & X_1 & X_2 & X_3 \end{bmatrix}_{z=d}^{\mathrm{T}}. \tag{31}$$

We can write it in the following form:

$$\begin{bmatrix} D_{11} & D_{12} \\ D_{21} & D_{22} \\ D_{31} & D_{32} \\ D_{41} & D_{42} \\ D_{51} & D_{52} \end{bmatrix}\begin{bmatrix} p \\ v_z \end{bmatrix}_{z=0} = \begin{bmatrix} R_{11} & R_{12} & R_{13} & R_{14} & R_{15} \\ 0 & R_{22} & R_{23} & R_{24} & R_{25} \\ 0 & 0 & R_{33} & R_{34} & R_{35} \\ 0 & 0 & 0 & R_{44} & R_{45} \\ 0 & 0 & 0 & 0 & R_{55} \end{bmatrix}\begin{bmatrix} p \\ v_z \\ X_1 \\ X_2 \\ X_3 \end{bmatrix}_{z=d}, [D]_{5\times2} = [Q]_{5\times5}^{\mathrm{H}}\left|\begin{matrix} 1 & 0 \\ 0 & 1 \\ \hline [0] & \end{matrix}\right|. \tag{32}$$

Expanding Equation (32) can obtain the expressions for X_1, X_2, and X_3 in terms of other parameters, and then substituting these three expressions back into the first and second lines of Equation (32):

$$\begin{aligned} &D_{11}p_0 + D_{12}v_{z0} = R_{11}p_d + R_{12}v_{zd} + R_{13}\left[\left(\frac{D_{31}}{R_{33}} + \frac{R_{34}D_{45}D_{51}}{R_{33}R_{44}R_{55}} - \frac{R_{34}D_{41}}{R_{33}R_{44}} - \frac{R_{35}D_{51}}{R_{33}R_{55}}\right)p_0 + \right. \\ &\left.\left(\frac{D_{32}}{R_{33}} + \frac{R_{34}R_{45}D_{52}}{R_{33}R_{44}R_{55}} - \frac{R_{34}D_{42}}{R_{33}R_{44}} - \frac{R_{35}D_{52}}{R_{33}R_{55}}\right)v_{z0}\right] + \\ &R_{14}\left[\left(\frac{D_{41}}{R_{44}} - \frac{R_{45}D_{51}}{R_{44}R_{55}}\right)p_0 + \left(\frac{D_{42}}{R_{44}} - \frac{R_{45}D_{52}}{R_{44}R_{55}}\right)v_{z0}\right] + R_{15}\left[\frac{D_{51}}{R_{55}}p_0 + \frac{D_{52}}{R_{55}}v_{z0}\right] \\ &D_{21}p_0 + D_{22}v_{z0} = R_{22}v_{zd} + R_{23}\left[\left(\frac{D_{31}}{R_{33}} + \frac{R_{34}D_{45}D_{51}}{R_{33}R_{44}R_{55}} - \frac{R_{34}D_{41}}{R_{33}R_{44}} - \frac{R_{35}D_{51}}{R_{33}R_{55}}\right)p_0 + \right. \\ &\left.\left(\frac{D_{32}}{R_{33}} + \frac{R_{34}R_{45}D_{52}}{R_{33}R_{44}R_{55}} - \frac{R_{34}D_{42}}{R_{33}R_{44}} - \frac{R_{35}D_{52}}{R_{33}R_{55}}\right)v_{z0}\right] + \\ &R_{24}\left[\left(\frac{D_{41}}{R_{44}} - \frac{R_{45}D_{51}}{R_{44}R_{55}}\right)p_0 + \left(\frac{D_{42}}{R_{44}} - \frac{R_{45}D_{52}}{R_{44}R_{55}}\right)v_{z0}\right] + R_{25}\left[\frac{D_{51}}{R_{55}}p_0 + \frac{D_{52}}{R_{55}}v_{z0}\right] \end{aligned}, \tag{33}$$

Finally, we can express Equation (33) in the form of Equation (12), with a total transfer matrix of $[T] = [E]_{2\times2}^{-1}\begin{bmatrix} R_{11} & R_{12} \\ 0 & R_{22} \end{bmatrix}$. The elements of the matrix $[E]$ are included in Appendix C.

The sound pressure and velocity that take into account the reflection and transmission of sound waves can be expressed by reflection and transmission coefficients. In other words, we can substitute the sound velocity and pressure in Equation (12) with reflection and transmission coefficients to facilitate our further solution of the sound absorption characteristics of the structure.

$$\begin{bmatrix} 1+RC \\ (1-RC)\cos\theta/(\rho_0 c_0) \end{bmatrix}_{z=0} = [T]_{2\times 2} \begin{bmatrix} TCe^{-ik_z d_s} \\ TCe^{-ik_z d_s}\cos\theta/(\rho_0 c_0) \end{bmatrix}_{z=d}, \tag{34}$$

where d_s is the thickness of the entire structure and k_z is the normal wave number component of the incident wave. ρ_0 and c_0 are the density of air and the speed of sound in air, respectively. Solving Equation (34) yields the reflection coefficient RC and the transmission coefficient TC.

$$TC = \frac{2\cos\theta/(\rho_0 c_0)}{e^{-ik_z d_s|_{z=d}}[T_{21} + (T_{11} + T_{22} + T_{12}\cos\theta/(\rho_0 c_0))\cos\theta/(\rho_0 c_0)]}, \tag{35}$$

$$RC = TC[T_{11} + T_{12}\cos\theta/(\rho_0 c_0)]e^{-ik_z d_s|_{z=d}} - 1\,. \tag{36}$$

Further, the absorption coefficient AC and the transmission loss TL of the structure can be calculated as follows:

$$AC = 1 - |RC|^2, \;\; TL = 10\log_{10}^{(1/|TC|^2)}, \tag{37}$$

The advantage of MTMM is its flexibility in handling the transfer matrix of material layers with different numbers of waves placed together. When the top and bottom of the porous elastic plate are bonded with a solid elastic plate, as shown in Figure 2, the matrices $[M_1]$, $[N_1]$, $[M_2]$, and $[N_2]$ are as follows [34]:

$$[M_1] = \begin{bmatrix} 0 & i\omega & 0 & 0 & 0 & 0 & 0 & 0 \\ 0 & 0 & 0 & i\omega & 0 & 0 & 0 & 0 \\ 0 & 0 & 0 & 0 & 0 & i\omega & 0 & 0 \\ 0 & -ik_x h_p/2 & 0 & 0 & 0 & 0 & 1/\left(D_p k_x^2 - m_s\omega^2\right) & 1 \\ 1 & Dk_x^4 - m_s\omega^2 & 1 & 0 & 1 & 0 & ik_x h_p/2 & 0 \end{bmatrix}, \; [N_1] = \begin{bmatrix} 0 & 1 \\ 0 & 1 \\ 0 & 1 \\ 0 & 0 \\ -1 & 0 \end{bmatrix}, \tag{38}$$

$$[M_2] = \begin{bmatrix} 0 & i\omega & 0 & 0 & 0 & 0 & 0 & 0 \\ 0 & 0 & 0 & i\omega & 0 & 0 & 0 & 0 \\ 0 & 0 & 0 & 0 & 0 & i\omega & 0 & 0 \\ 0 & ik_x h_p/2 & 0 & 0 & 0 & 0 & 1/\left(\omega^2 m_s - D_p k_x^2\right) & 1 \\ -1 & Dk_x^4 - m_s\omega^2 & -1 & 0 & -1 & 0 & ik_x h_p/2 & 0 \end{bmatrix}, \; [N_2] = \begin{bmatrix} 0 & 1 \\ 0 & 1 \\ 0 & 1 \\ 0 & 0 \\ 1 & 0 \end{bmatrix}, \tag{39}$$

where k_x represents the wave number component in the x direction, h_p is the thickness of the solid panel, and $m_s = \rho_p h_p$ is the panel mass per unit area. $D = h_p^3 E_p\left(1 + i\eta_p\right)/12\left(1 - \nu_p^2\right)$ is the panel flexural stiffness per unit width, and $D_p = E_p h_p$ is the panel longitudinal stiffness per unit width. We perform a dimensionality reduction and dimensionality increase on the matrices in Equation (36) similar to that in the previous content, which allows us to relate the state vectors in the air on both sides of the structure and further obtain the sound absorption properties.

In Figure 3, when a single solid elastic plate is bonded over the porous elastic layer, the elements in the matrices $[M_1]$ and $[N_1]$ are the same as those of the unsaturated porous plate when it is bonded with solid plates on both the upper and lower sides. On the other hand, the matrices $[M_2]$ and $[N_2]$ are consistent with the elastic plate in the absence of bonding, that is, when it is exposed to air.

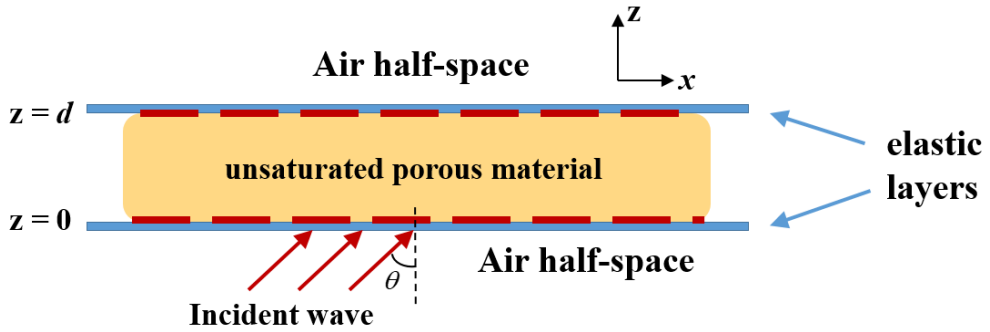


Figure 2. Sound wave incident into an unsaturated porous elastic plate bonded with solid layers on both upper and lower surfaces.

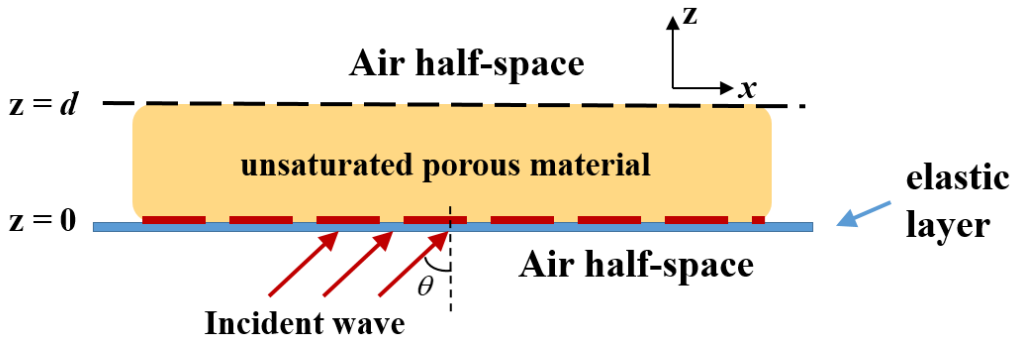


Figure 3. Sound wave incident into an unsaturated porous elastic plate bonded with a solid layer on the bottom.

When only one solid elastic version is bonded to the lower layer of the porous elastic layer, as shown in Figure 4, the matrices $[M_1]$ and $[N_1]$ are the same as when the elastic plate is exposed to air. The matrices $[M_2]$ and $[N_2]$ are consistent with the unsaturated porous plate when it is bonded with solid plates on both the upper and lower sides.

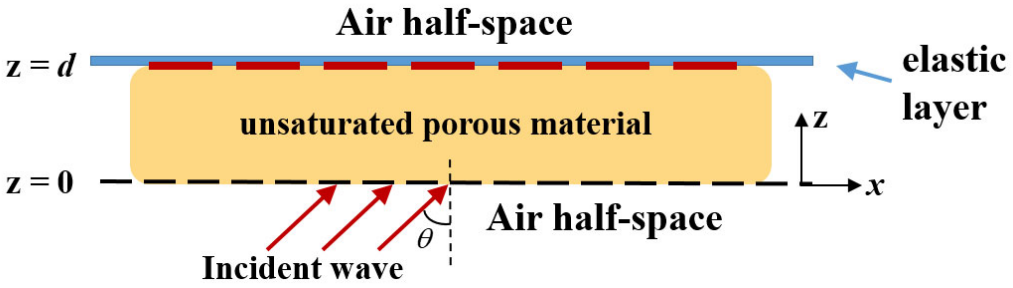


Figure 4. Sound wave incident into an unsaturated porous elastic plate bonded with a solid layer on top.

4. Results and Discussion

The physical characteristics and structural properties of unsaturated porous materials play a significant role in determining their sound absorption properties, much like saturated porous materials. In this section, we use the method introduced in the previous section to numerically calculate and compare the sound absorption properties of an unsaturated porous elastic plate under various parameter settings. The air density on either side of the unsaturated porous plate is $\rho_0 = 1.21\ \mathrm{kg/m^3}$, while the speed of sound in the air is $c_0 = 343\ \mathrm{m/s}$. The parameters used to characterize the unsaturated porous plate are those of sandstone filled with water and carbon dioxide from [21]: The parameters characterizing the unsaturated porous plate are as follows: $\rho_s = 2650\ \mathrm{kg/m^3}$, $\rho_g = 103\ \mathrm{kg/m^3}$, $\rho_l = 990\ \mathrm{kg/m^3}$, $K_b = 6.5 \times 10^{10}\ \mathrm{Pa}$, $K_g = 3.7 \times 10^6\ \mathrm{Pa}$, $K_l = 2.3 \times 10^9\ \mathrm{Pa}$,

$G = 4.8 \times 10^{10}$ Pa, and $dP_c/dS_g = 0.05 \times 10^6$ in order to improve the practicality of this study in building sound insulation. The values chosen for the dissipation coefficient are $d_g = 0.04 \times 10^4$ Pa · s/m^2 and $d_l = 1 \times 10^4$ Pa · s/m^2.The material parameters of the solid elastic plate bonded to the porous plate are $E_p = 7 \times 10^9$ Pa, $\nu_p = 0.33$, $\rho_p = 2700$ kg/m^3, $h_p = 0.003$ m, and $\eta_p = 0.003$.

Figures 5–8 illustrate the sound absorption characteristics of the unsaturated porous elastic plate exposed to air under various parameter conditions. The subplot (a) in each figure displays the absorption coefficient, while the subplot (b) shows the transmission loss. The parameters examined include plate thickness, porosity, saturation, and the incident angle of the acoustic wave. Figures 9–12 illustrate the sound absorption properties of an unsaturated porous elastic plate that is bonded with solid elastic plates on both the upper and lower ends. Figures 13–16 contrast the situations where a solid elastic plate is respectively bonded at the upper and lower ends of an unsaturated porous elastic plate.

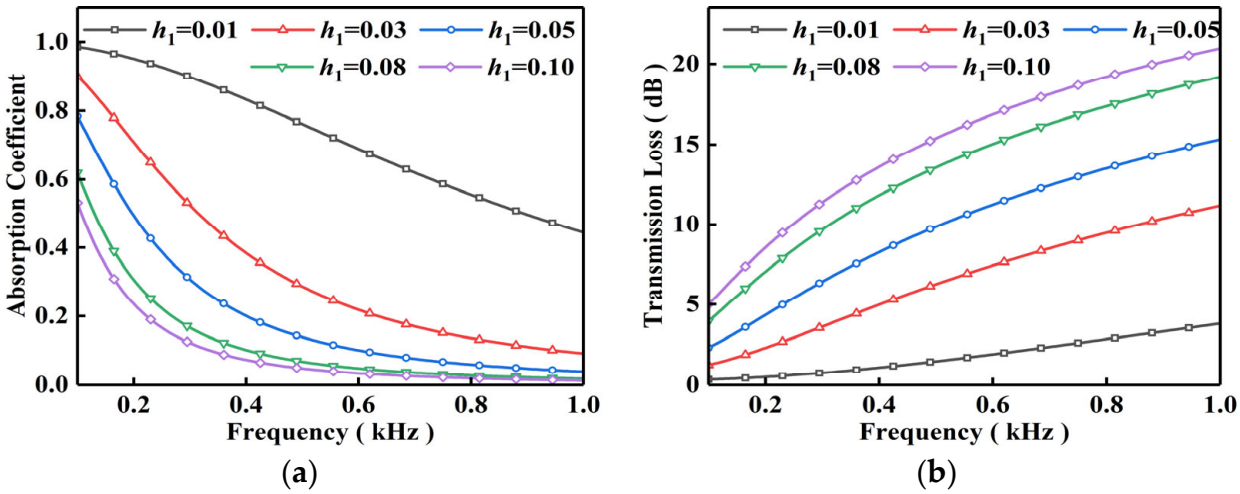


Figure 5. Sound absorption properties of an unsaturated elastic plate exposed to air with different thicknesses: (**a**) absorption coefficient and (**b**) transmission loss.

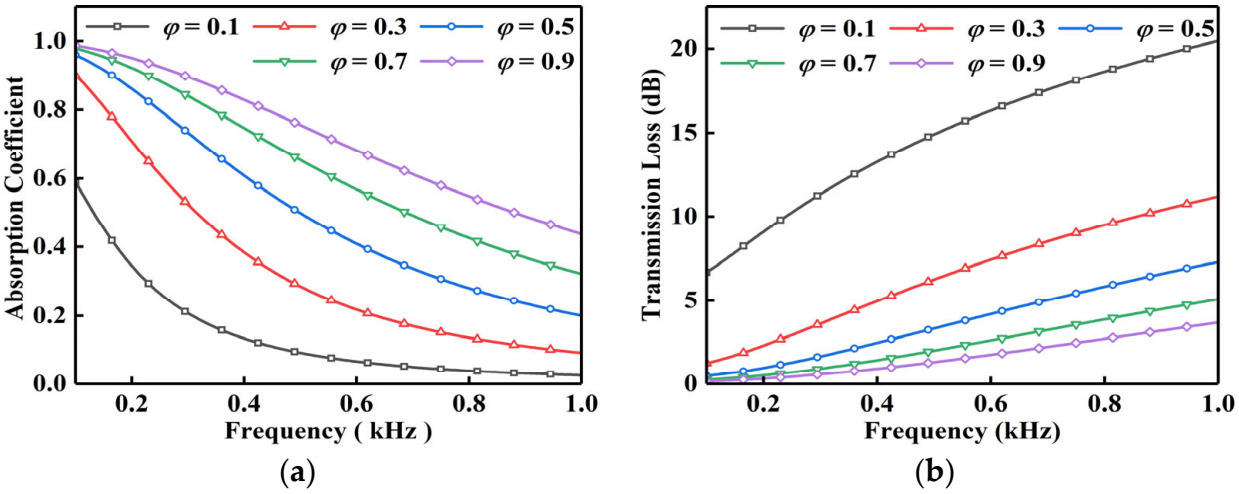


Figure 6. Sound absorption properties of an unsaturated elastic plate exposed to air with different porosities: (**a**) absorption coefficient and (**b**) transmission loss.

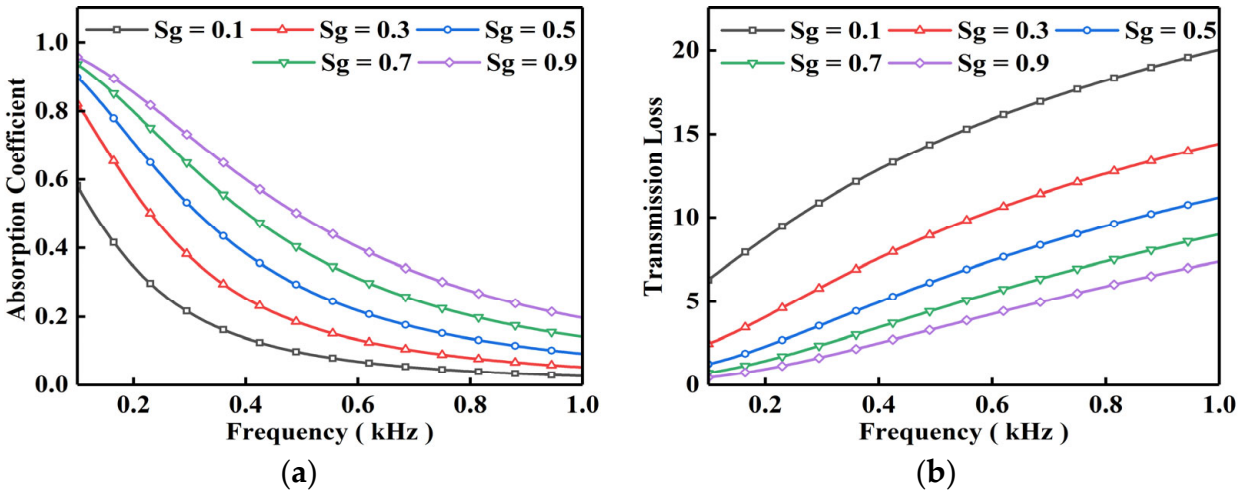


Figure 7. Sound absorption properties of an unsaturated elastic plate exposed to air with different gas saturations: (**a**) absorption coefficient and (**b**) transmission loss.

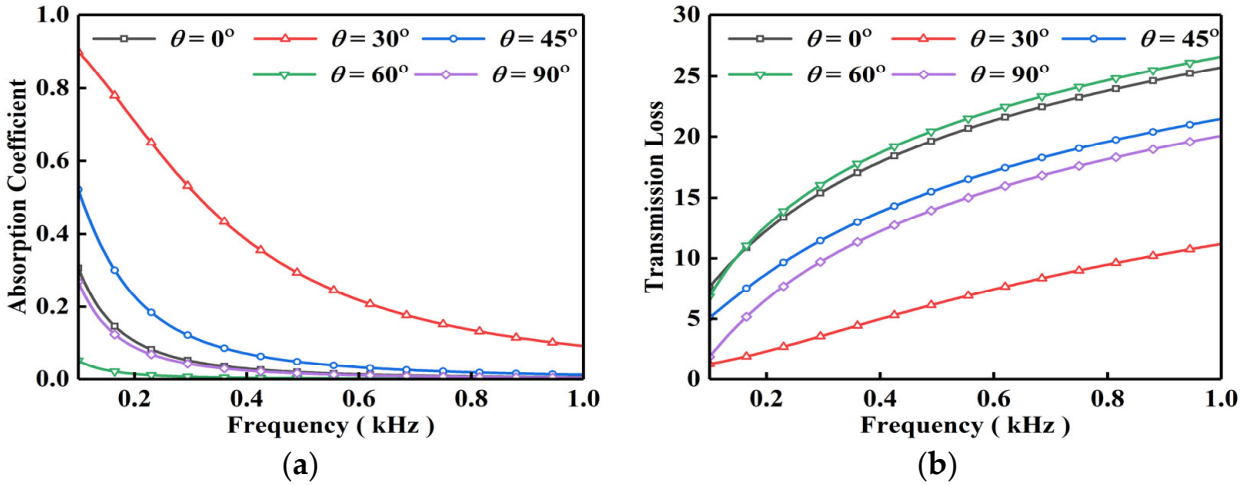


Figure 8. Sound absorption properties of an unsaturated elastic plate exposed to air at different incident angles of sound wave: (**a**) absorption coefficient and (**b**) transmission loss.

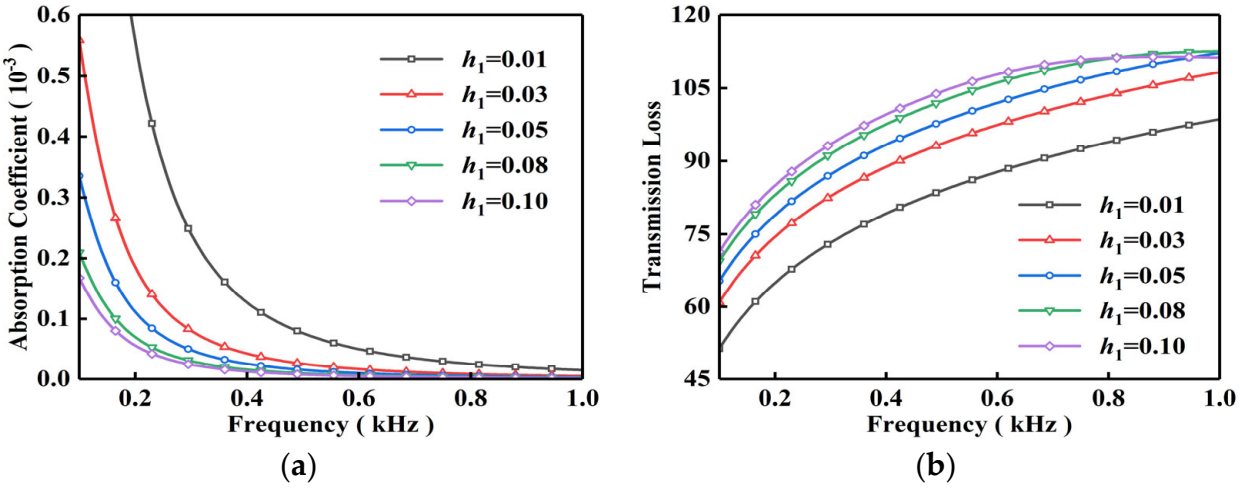
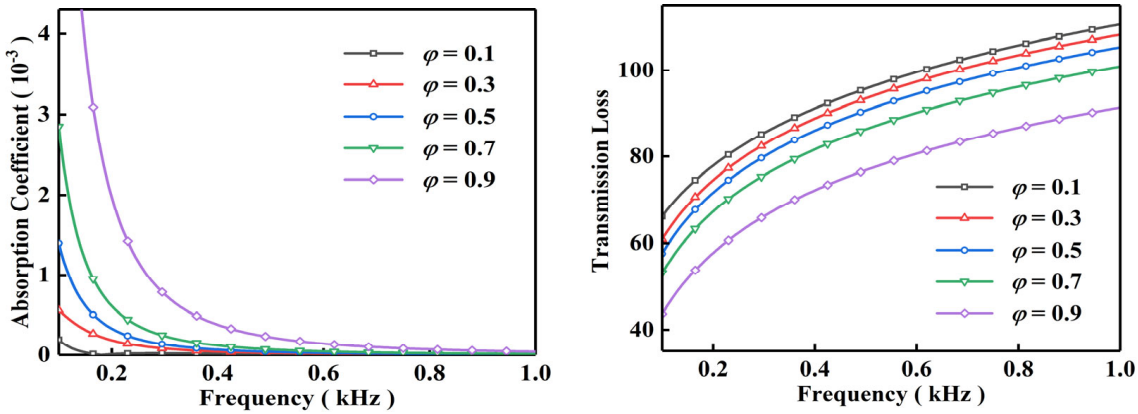
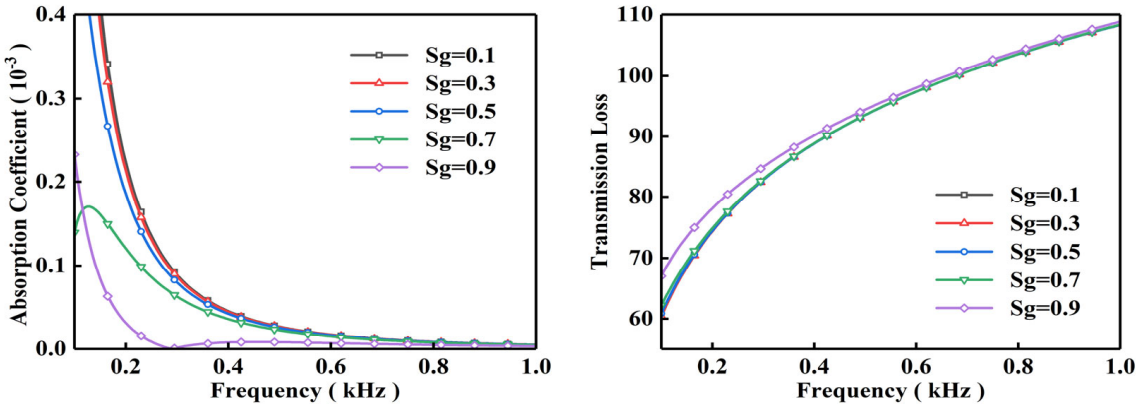


Figure 9. Sound absorption characteristics of unsaturated porous elastic plates with solid elastic plates bonded at both the top and bottom of different thicknesses: (**a**) absorption coefficient and (**b**) transmission loss.



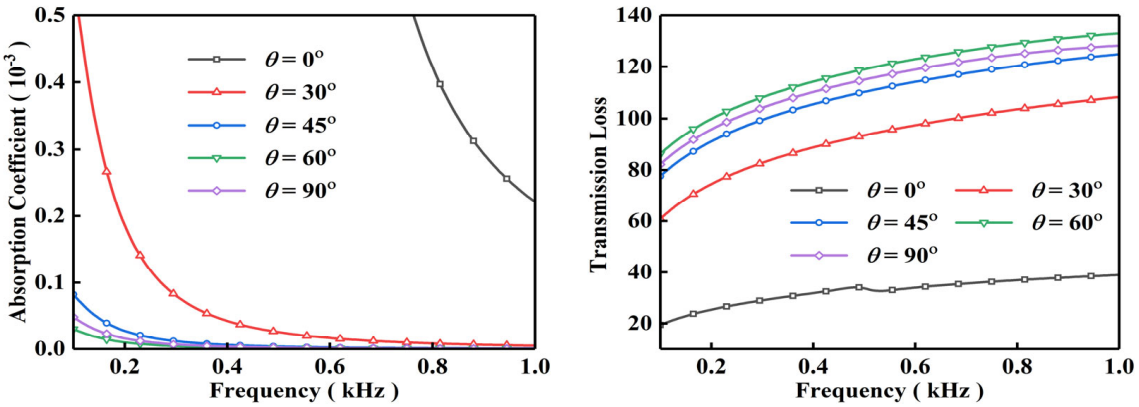
(**a**) (**b**)

Figure 10. Sound absorption characteristics of an unsaturated porous elastic plate with solid elastic plates bonded at both the top and bottom of different porosities: (**a**) absorption coefficient and (**b**) transmission loss.



(**a**) (**b**)

Figure 11. Sound absorption characteristics of an unsaturated porous elastic plate with solid elastic plates bonded at both the top and bottom of different saturations: (**a**) absorption coefficient and (**b**) transmission loss.



(**a**) (**b**)

Figure 12. Sound absorption characteristics of an unsaturated porous elastic plate with solid elastic plates bonded at both the top and bottom of different incident angles of sound wave: (**a**) absorption coefficient and (**b**) transmission loss.

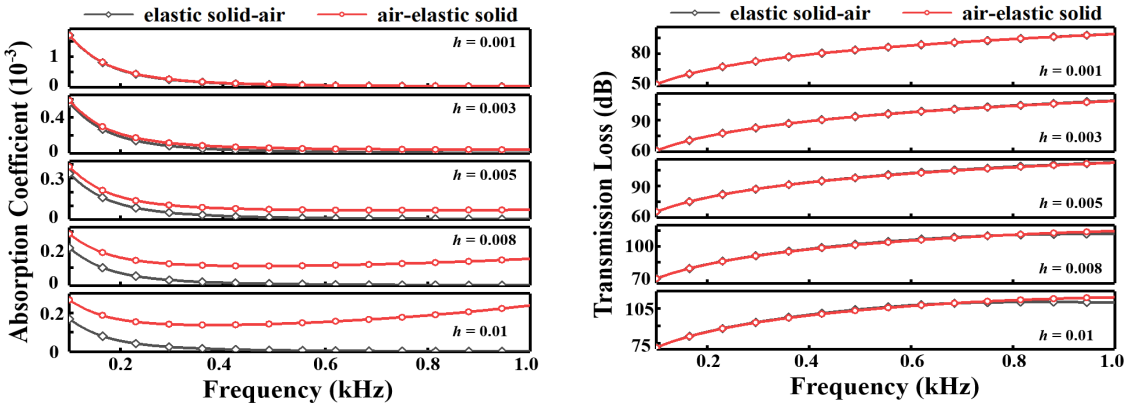


Figure 13. Sound absorption properties of an unsaturated porous elastic plate when bonded with a solid elastic plate on top and bottom, respectively, at different thicknesses: (**a**) absorption coefficient and (**b**) transmission loss.

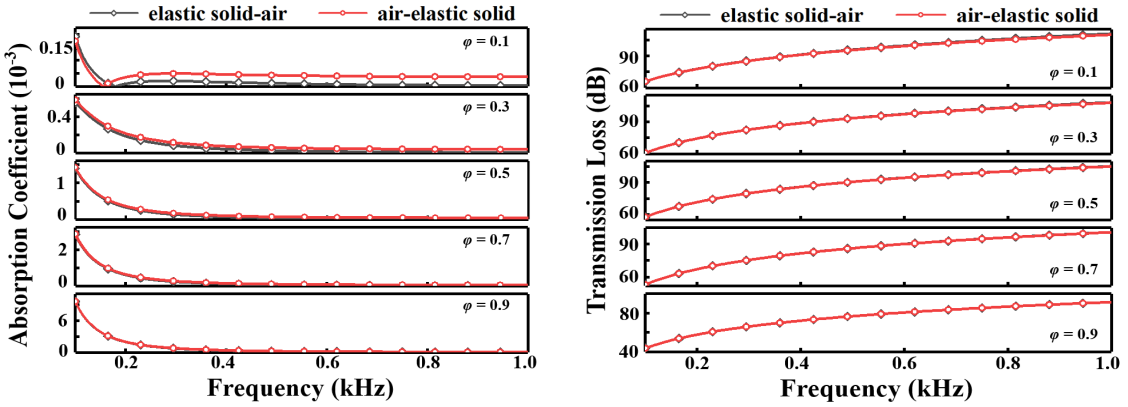


Figure 14. Sound absorption properties of an unsaturated porous elastic plate when bonded with a solid elastic plate on top and bottom, respectively, at different porosities: (**a**) absorption coefficient and (**b**) transmission loss.

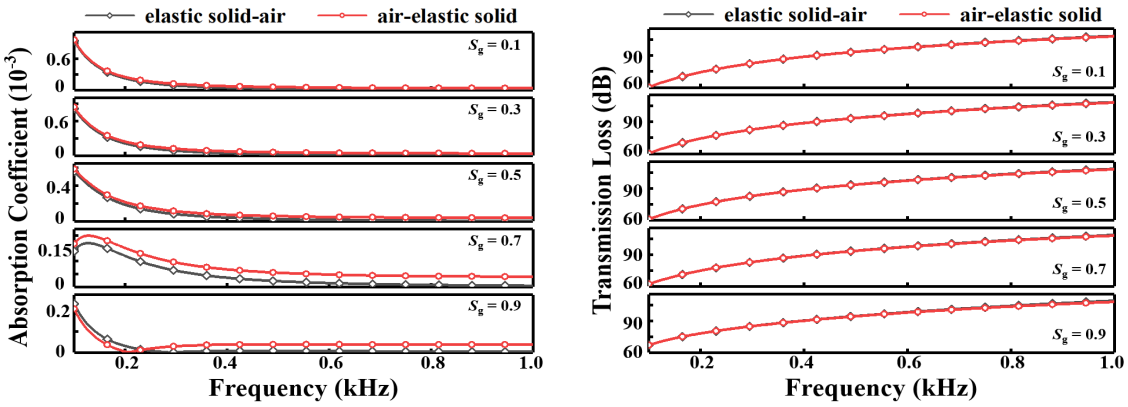


Figure 15. Sound absorption properties of an unsaturated porous elastic plate when bonded with a solid elastic plate on top and bottom, respectively, at different saturations: (**a**) absorption coefficient and (**b**) transmission loss.

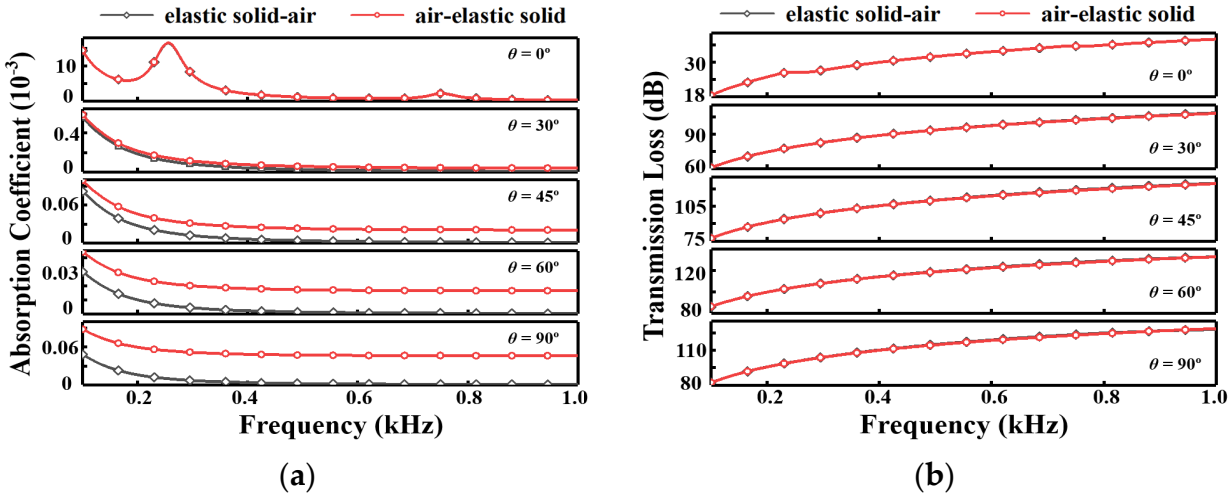


Figure 16. Sound absorption properties of an unsaturated porous elastic plate when bonded with a solid elastic plate on top and bottom, respectively, at different incident angles of the sound wave: (**a**) absorption coefficient and (**b**) transmission loss.

Figure 5 illustrates the sound absorption characteristics of the unsaturated porous elastic plate with varying thicknesses exposed to air. As shown in Figure 5a, the absorption coefficient decreases with increasing frequency, and the rate of decrease is slower for thinner plates. As the thickness of the elastic plate increases, the absorption coefficient gradually decreases, and the rate of decrease with frequency becomes greater. In contrast to the trend observed for the absorption coefficient, Figure 5b shows that the transmission loss of the unsaturated porous elastic plate increases with frequency and plate thickness. For plate thicknesses ranging from 0.01 to 0.1 m, the transmission loss of the unsaturated porous elastic plate exposed to air is between 0 and 20 dB. Compared with fluid-saturated porous materials of the same thickness, unsaturated porous materials have added gas to their pores, allowing them to flow with the air on both sides of the porous material plate, reducing the absorption coefficient and transmission loss of the structure.

Figure 6 shows the sound absorption characteristics of unsaturated porous elastic plates exposed to air with different porosities. As shown in Figure 6a, the absorption coefficient increases with increasing porosity. When the porosity is greater than 0.5 and the frequency is 0.1 kHz, the absorption coefficient approaches 1. However, when the porosity is reduced to 0.1, the absorption coefficient is approximately 0.6. As demonstrated in Figure 6b, when the porosity is held constant, the transmission loss increases with frequency, with the most significant change observed when the porosity is small. As porosity increases, the transmission loss decreases, ranging from 5 to 20 dB for a porosity of 0.1 and 0 to 13 dB for other selected porosity settings.

Figure 7a,b show the absorption coefficients and transmission losses of unsaturated porous elastic plates with different gas saturations, respectively. Similar to the previous parameters, the dependence of the absorption coefficient and transmission loss on frequency and saturation is opposite. Specifically, the absorption coefficient increases with increasing saturation, and the transmission loss decreases.

Figure 8 illustrates that there is no definitive pattern for the effect of the incidence angle of the acoustic wave on the absorption parameters (absorption coefficient and transmission loss) of unsaturated porous elastic plates when exposed to air.

Figures 9–12 depict the sound absorption properties of an unsaturated porous elastic plate that is bonded with solid elastic plates on both the upper and lower ends, and we can compare and analyze these findings with the results shown in Figures 5–8 that were obtained from the porous plate exposed to air. Overall, unsaturated porous materials bonded with elastic plates at both ends exhibit extremely low absorption coefficients and significantly increased transmission losses. This is because the coupling between liquid and gas in the pores increases the transmission losses of unsaturated porous materials when

both ends are isolated from air. The combination with the elastic plate further in-creases the transmission loss of the structure. From a numerical perspective, the transmission loss of the structure with added elastic plates at higher frequencies is about 5–6 times that of unsaturated porous material plates exposed to air, which is consistent with the results in reference [32] and to some extent supports the correctness of this paper. In Figure 9a, it can be observed that the absorption coefficient decreases rapidly with increasing frequency at lower frequencies and slows down at higher frequencies. Additionally, as the thickness of the porous plate increases, the absorption coefficient decreases. Overall, the absorption coefficient of the porous elastic plate with solid elastic plates bonded at both the upper and lower ends is three orders of magnitude lower than that of the porous elastic plate exposed to air. On the other hand, in Figure 9b, it can be observed that the transmission loss is significantly higher than that of the porous elastic plate exposed to air, with a range of 40–120 dB. The transmission loss increases with an increase in the frequency and thickness of the plate.

Figure 10a demonstrates that the absorption coefficient of the unsaturated porous elastic plate increases with porosity. At a porosity of 0.1, the absorption coefficient is close to zero across all frequencies, but with an increase in porosity, the absorption coefficient notably surpasses zero. In Figure 10b, it can be observed that the transmission loss decreases as porosity increases. Additionally, the rate of change of transmission loss with frequency is similar for different porosity conditions.

Figure 11a illustrates the impact of saturation on the absorption coefficient of an unsaturated porous elastic plate with solid elastic plates bonded at both the upper and lower ends. A saturation of 0.5 appears to be a critical point, where saturation has little effect on the absorption coefficient when it is below 0.5. However, when the saturation exceeds 0.5, the absorption coefficient decreases significantly with increasing saturation. Furthermore, the transmission loss also shows a more pronounced change at saturations greater than 0.5, with an increasing trend as saturation increases, as depicted in Figure 11b.

Figure 12 displays the sound absorption properties for various sound wave incident angles. Among the chosen incidence angles, it can be observed that the absorption co-efficient decreases as the incidence angle increases when the incident angle is less than 60 degrees. And the transmission loss increases as the incident angle increases.

Figures 13–16 present a comparison of the sound absorption performance when the solid elastic plate is bonded above and below the porous elastic plate, respectively. The black curve corresponds to the case when the solid elastic plate is bonded below the porous plate, whereas the red curve represents the scenario where the solid plate is bonded on top. As depicted in Figure 13a, the position of the solid elastic plate has a significant impact on the absorption coefficient, especially when the thickness of the porous elastic plate is larger. In general, as the thickness of the porous plate increases, the absorption coefficient in both cases decreases; however, when the solid plate is bonded below the porous plate, the absorption coefficient decreases at a faster rate than when the solid plate is on top. Therefore, as the thickness of the porous plate increases, the difference in the absorption coefficient between the two cases becomes increasingly apparent. Specifically, when a solid plate is on top of a porous plate, the absorption coefficient of the structure is higher than when the solid plate is below the porous plate, and this difference grows as the thickness of the porous plate increases. As for Figure 13b, the transmission loss increases as the thickness of the porous plate increases, and the difference in both cases also becomes more significant with the increase in thickness. Additionally, when only one side of the structure is bonded with a solid plate, the sound absorption characteristics of the structure are not significantly different from when both sides are bonded with a solid plate.

As shown in Figure 14a, the absorption coefficient generally increases with the increasing porosity of the porous plate, which is consistent with the findings from the previous two scenarios. Moreover, when the solid plate is positioned above the porous plate, the absorption coefficient tends to be higher than when the solid plate is located below, except for cases where the porosity is 0.1 and the frequency is very low. However, this difference

gradually decreases as the porosity of the porous plate increases. In Figure 14b, it can be observed that the transmission loss decreases as the porosity increases, and the position of the solid plate in relation to the porous plate does not seem to have a significant impact on the transmission loss.

The impact of saturation on sound absorption properties is shown in Figure 15. When the solid plate is bonded either above or below the porous plate, the transmission losses are quite similar. However, as the saturation level increases, there are significant differences in the absorption coefficients, which tend to be higher when the solid plate is positioned above the porous plate compared to when it is positioned below the porous plate.

In both scenarios, the absorption coefficient tends to decrease as the incidence angle increases up to 60 degrees. When the solid plate is bonded above the porous plate, the absorption coefficient is consistently higher than when the solid plate is below, and this difference between the two situations becomes more significant as the incidence angle increases. The transmission loss shows an opposite trend to the absorption coefficient, and the values are comparable in the two circumstances. In order to more intuitively demonstrate the sound absorption characteristics of structures under different conditions, the total numerical range of their absorption coefficient and transmission loss under different parameter conditions are listed in the Table 1 below.

Table 1. Absorption coefficient and projection loss range for different situations.

Different Conditions	AC Min	AC Max	TL Min	TL Max
Exposed to the air	0	1	0	27
Elastic plates bonded at both sides	0	6×10^{-3}	0	132
Elastic plates bonded at one side	0	1.5×10^{-3}	18	125

5. Conclusions

A modified transfer matrix approach is introduced in the problem of sound absorption by unsaturated porous materials, and the approach is applied to calculate the sound absorption properties of unsaturated porous elastic plates under different cases for exposed to air and bonded solid elastic plates. We have chosen sandstone with pores filled with water and carbon dioxide as the simulation object, which can be used as an excellent building material for external wall construction or indoor decoration when bonded with elastic plates. This undoubtedly provides some reference for the application of unsaturated porous materials to sound absorption in buildings. In addition, we also investigated and discussed the influence of different structural parameters on the sound absorption performance, providing theoretical support for optimizing the sound absorption performance of this structure.

When a solid elastic plate is bonded over an unsaturated porous elastic plate, the transmission loss is substantially increased in comparison to a single unsaturated porous elastic plate exposed to air. When the solid plate is bonded above the porous plate, the absorption coefficient and transmission loss are similar to those of the porous plate with two solid plates bonded at both upper and lower ends. However, when the solid plate is bonded below the porous plate, the absorption coefficient is slightly smaller than in the previous cases, while the transmission losses are comparable. The impact of unsaturated porous elastic plate thickness, porosity, and saturation on structural absorption properties is consistent across different structures. Specifically, reducing the thickness, increasing the porosity, and increasing the saturation of the unsaturated porous elastic plate result in an increase in the absorption coefficient and a decrease in transmission loss. Furthermore, when these parameters reach larger values, the sound absorption performance of materials exhibits more pronounced variations with frequency.

It is worth noting that the sound absorption results of unsaturated porous materials bonded to elastic plates are better than those of saturated porous materials. Therefore, in practical construction projects, artificial gas–liquid replacement can be considered for some fluids of fluid-saturated porous materials to achieve better sound absorption effects. The study on the influence of material parameters on the results in this article also provides theoretical support

for the practical application of performance optimization of building materials. However, this study still has some limitations. First, the simulated frequency range is small, while there are many types of noise in reality, and the frequency range is wide. Therefore, further research is needed to obtain a universal conclusion. Second, the application of the modified transfer matrix method between material layers with the same number of wavenumbers is cumbersome, and further improvement is needed to apply this method to all materials. Finally, we only discussed the impact of individual material parameters on the results, and in subsequent work, coupling parameters needed to be considered.

Author Contributions: Y.Y.: data curation, writing—original draft, methodology, software. W.G.: conceptualization, supervision, writing—review and editing, project administration, funding acquisition. All authors have read and agreed to the published version of the manuscript.

Funding: Wei Guan was supported by the National Natural Science Foundations of China (Nos. 41874129, 11972132, and 12272107).

Data Availability Statement: The datasets used and/or analyzed during the current study are available from the authors upon reasonable request. The data are not publicly available due to privacy.

Conflicts of Interest: The authors declared no potential conflicts of interest with respect to the research, authorship, and/or publication of this article.

Appendix A

List of symbols

ϕ_s, ϕ_l, ϕ_g	the volume fractions of the solid, liquid, and gas phases
S_l, S_g	relative saturation of the liquid and gas phases
τ_s, τ_l, τ_g	stress of the solid, liquid, and gas phases (Pa)
τ	total stress (Pa)
μ	shear modulus of the solid frame (Pa)
ε	strain
u	displacement (m)
K_b, K_l, K_g	the bulk modulus of the porous frame, liquid, and gas phases (Pa)
P_c	the function describing the capillary pressure
α_{vg}, m_{vg}	the van Genuchten model parameters
ρ_s, ρ_l, ρ_g	density of solid grain, liquid, and gas phases (kg/m^3)
d_l, d_g	the coefficients related to viscous drag
κ_{rl}, κ_{rg}	the relative permeability of the liquid and gas phases
κ_s	absolute permeability of the unsaturated porous material (μm^2)
η_l, η_g	the dynamic shear viscosities of the liquid and gas phases (Pa $\cdot$ s)
θ	incident angle (^{o})
p	sound pressure (Pa)
v_z	sound velocity (m/s)
ω	frequency (Hz)
d_s	the thickness of the entire structure (m)
k_z, k_x	wavenumber in the z and x directions, respectively
ρ_0	the density of air (kg/m^3)
c_0	the speed of sound in air (m/s)
TC	transmission coefficient
RC	reflection coefficient
AC	absorption coefficient
TL	transmission loss
m_s	the mass per unit area of the elastic plate (kg)
h_p	thickness of the elastic plate (m)
D_p	the flexural and longitudinal stiffnesses of the elastic plate (N/m)
ρ_p	the density of the elastic plate (kg/m^3)
E_p	the Young's modulus of the elastic plate (Pa)
ν_p	the Poisson's ratio of the elastic plate
η_p	loss factor of the elastic plate

Appendix B

The elements of the matrix $[C]$ are as follows:

$$c_{11} = \left[-2\mu k_{p1z}^2 + \left(\frac{2\mu}{3} - a_{11} - a_{12}A_{g1} - a_{13}A_{l1}\right)\left(k_{p1z}^2 + k_{px}^2\right)\right]\cos(k_{p1z}z)$$

$$c_{12} = i\left[-2\mu k_{p1z}^2 + \left(\frac{2\mu}{3} - a_{11} - a_{12}A_{g1} - a_{13}A_{l1}\right)\left(k_{p1z}^2 + k_{px}^2\right)\right]\sin(k_{p1z}z)$$

$$c_{13} = \left[-2\mu k_{p2z}^2 + \left(\frac{2\mu}{3} - a_{11} - a_{12}A_{g2} - a_{13}A_{l2}\right)\left(k_{p2z}^2 + k_{px}^2\right)\right]\cos(k_{p2z}z)$$

$$c_{14} = i\left[-2\mu k_{p2z}^2 + \left(\frac{2\mu}{3} - a_{11} - a_{12}A_{g2} - a_{13}A_{l2}\right)\left(k_{p2z}^2 + k_{px}^2\right)\right]\sin(k_{p2z}z)$$

$$c_{15} = \left[-2\mu k_{p3z}^2 + \left(\frac{2\mu}{3} - a_{11} - a_{12}A_{g3} - a_{13}A_{l3}\right)\left(k_{p3z}^2 + k_{px}^2\right)\right]\cos(k_{p3z}z)$$

$$c_{16} = i\left[-2\mu k_{p3z}^2 + \left(\frac{2\mu}{3} - a_{11} - a_{12}A_{g3} - a_{13}A_{l3}\right)\left(k_{p3z}^2 + k_{px}^2\right)\right]\sin(k_{p3z}z)$$

$$c_{17} = -2i\mu k_{sz}k_{px}\sin(k_{sz}z)\ c_{18} = -2\mu k_{sz}k_{px}\cos(k_{sz}z)$$

$$c_{21} = -k_{p1z}\sin(k_{p1z}z)\ c_{22} = ik_{p1z}\cos(k_{p1z}z)\ c_{23} = -k_{p2z}\sin(k_{p2z}z)\ c_{24} = ik_{p2z}\cos(k_{p2z}z)$$

$$c_{25} = -k_{p3z}\sin(k_{p3z}z)\ c_{26} = ik_{p3z}\cos(k_{p3z}z)\ c_{27} = ik_{px}\cos(k_{sz}z)\ c_{28} = -k_{px}\sin(k_{sz}z)$$

$$c_{31} = -\left(a_{21} + a_{22}A_{g1} + a_{23}A_{l1}\right)\left(k_{p1z}^2 + k_{px}^2\right)\cos(k_{p1z}z)$$

$$c_{32} = -i\left(a_{21} + a_{22}A_{g1} + a_{23}A_{l1}\right)\left(k_{p1z}^2 + k_{px}^2\right)\sin(k_{p1z}z)$$

$$c_{33} = -\left(a_{21} + a_{22}A_{g2} + a_{23}A_{l2}\right)\left(k_{p2z}^2 + k_{px}^2\right)\cos(k_{p2z}z)$$

$$c_{34} = -i\left(a_{21} + a_{22}A_{g2} + a_{23}A_{l2}\right)\left(k_{p2z}^2 + k_{px}^2\right)\sin(k_{p2z}z)$$

$$c_{35} = -\left(a_{21} + a_{22}A_{g3} + a_{23}A_{l3}\right)\left(k_{p3z}^2 + k_{px}^2\right)\cos(k_{p3z}z)$$

$$c_{36} = -i\left(a_{21} + a_{22}A_{g3} + a_{23}A_{l3}\right)\left(k_{p3z}^2 + k_{px}^2\right)\sin(k_{p3z}z)\ c_{37} = 0\ c_{38} = 0$$

$$c_{41} = -A_{g1}k_{p1z}\sin(k_{p1z}z)\ c_{42} = iA_{g1}k_{p1z}\cos(k_{p1z}z)\ c_{43} = -A_{g2}k_{p2z}\sin(k_{p2z}z)$$

$$c_{44} = iA_{g2}k_{p2z}\cos(k_{p2z}z)\ c_{45} = -A_{g3}k_{p3z}\sin(k_{p3z}z)\ c_{46} = iA_{g3}k_{p3z}\cos(k_{p3z}z)$$

$$c_{47} = iB_g k_{px}\cos(k_{sz}z)\ c_{48} = -B_g k_{px}\sin(k_{sz}z)$$

$$c_{51} = -\left(a_{31} + a_{32}A_{g1} + a_{33}A_{l1}\right)\left(k_{p1z}^2 + k_{px}^2\right)\cos(k_{p1z}z)$$

$$c_{52} = -i\left(a_{31} + a_{32}A_{g1} + a_{33}A_{l1}\right)\left(k_{p1z}^2 + k_{px}^2\right)\sin(k_{p1z}z)$$

$$c_{53} = -\left(a_{31} + a_{32}A_{g2} + a_{33}A_{l2}\right)\left(k_{p2z}^2 + k_{px}^2\right)\cos(k_{p2z}z)$$

$$c_{54} = -i\left(a_{31} + a_{32}A_{g2} + a_{33}A_{l2}\right)\left(k_{p2z}^2 + k_{px}^2\right)\sin(k_{p2z}z)$$

$$c_{55} = -\left(a_{31} + a_{32}A_{g3} + a_{33}A_{l3}\right)\left(k_{p3z}^2 + k_{px}^2\right)\cos(k_{p3z}z)$$

$$c_{56} = -i\left(a_{31} + a_{32}A_{g3} + a_{33}A_{l3}\right)\left(k_{p3z}^2 + k_{px}^2\right)\sin(k_{p3z}z)\ c_{57} = 0\ c_{58} = 0$$

$$c_{61} = -A_{l1}k_{p1z}\sin(k_{p1z}z)\ c_{62} = iA_{l1}k_{p1z}\cos(k_{p1z}z)\ c_{63} = -A_{l2}k_{p2z}\sin(k_{p2z}z)$$

$$c_{64} = iA_{l2}k_{p2z}\cos(k_{p2z}z)\ c_{65} = -A_{l3}k_{p3z}\sin(k_{p3z}z)\ c_{66} = iA_{l3}k_{p3z}\cos(k_{p3z}z)$$

$$c_{67} = iB_g k_{px}\cos(k_{sz}z)\ c_{68} = -B_g k_{px}\sin(k_{sz}z)$$

$$c_{71} = -2i\mu k_{p1z}k_{px}\sin(k_{p1z}z)\ c_{72} = -2\mu k_{p1z}k_{px}\cos(k_{p1z}z)\ c_{73} = -2i\mu k_{p2z}k_{px}\sin(k_{p2z}z)$$

$$c_{74} = -2\mu k_{p2z}k_{px}\cos(k_{p2z}z)\ c_{75} = -2i\mu k_{p3z}k_{px}\sin(k_{p3z}z)\ c_{76} = -2\mu k_{p3z}k_{px}\cos(k_{p3z}z)$$

$$c_{77} = -\mu\left(k_{px}^2 - k_{sz}^2\right)\cos(k_{sz}z)\ c_{78} = -i\mu\left(k_{px}^2 - k_{sz}^2\right)\sin(k_{sz}z)$$

$$c_{81} = ik_{px}\cos(k_{p1z}z)\ c_{82} = -k_{px}\sin(k_{p1z}z)\ c_{83} = ik_{px}\cos(k_{p2z}z)\ c_{84} = -k_{px}\sin(k_{p2z}z)$$

$$c_{85} = ik_{px}\cos(k_{p3z}z)\ c_{86} = -k_{px}\sin(k_{p3z}z)\ c_{87} = k_{sz}\sin(k_{sz}z)\ c_{88} = -ik_{sz}\cos(k_{sz}z)$$

Appendix C

The elements of the matrix $[E]$ are as follows:

$$X_1 = \left(\frac{D_{31}}{R_{33}} + \frac{R_{34}D_{45}D_{51}}{R_{33}R_{44}R_{55}} - \frac{R_{34}D_{41}}{R_{33}R_{44}} - \frac{R_{35}D_{51}}{R_{33}R_{55}}\right)p_0 + \left(\frac{D_{32}}{R_{33}} + \frac{R_{34}R_{45}D_{52}}{R_{33}R_{44}R_{55}} - \frac{R_{34}D_{42}}{R_{33}R_{44}} - \frac{R_{35}D_{52}}{R_{33}R_{55}}\right)v_{z0}$$

$$X_2 = \left(\frac{D_{41}}{R_{44}} - \frac{R_{45}D_{51}}{R_{44}R_{55}}\right)p_0 + \left(\frac{D_{42}}{R_{44}} - \frac{R_{45}D_{52}}{R_{44}R_{55}}\right)v_{z0}$$

$$X_3 = \frac{D_{51}}{R_{55}}p_0 + \frac{D_{52}}{R_{55}}v_{z0}$$

$$E_{11} = D_{11} - \left(\frac{R_{13}D_{31}}{R_{33}} + \frac{R_{13}R_{34}D_{45}D_{51}}{R_{33}R_{44}R_{55}} - \frac{R_{13}R_{34}D_{41}}{R_{33}R_{44}} - \frac{R_{13}R_{35}D_{51}}{R_{33}R_{55}}\right) - \left(\frac{R_{14}D_{41}}{R_{44}} - \frac{R_{14}R_{45}D_{51}}{R_{44}R_{55}}\right) - \frac{R_{15}D_{51}}{R_{55}}$$

$$E_{12} = D_{12} - \left(\frac{R_{13}D_{32}}{R_{33}} + \frac{R_{13}R_{34}D_{45}D_{52}}{R_{33}R_{44}R_{55}} - \frac{R_{13}R_{34}D_{42}}{R_{33}R_{44}} - \frac{R_{13}R_{35}D_{52}}{R_{33}R_{55}}\right) - \left(\frac{R_{14}D_{42}}{R_{44}} - \frac{R_{14}R_{45}D_{52}}{R_{44}R_{55}}\right) - \frac{R_{15}D_{52}}{R_{55}}$$

$$E_{21} = D_{21} - \left(\frac{R_{23}D_{31}}{R_{33}} + \frac{R_{23}R_{34}D_{45}D_{51}}{R_{33}R_{44}R_{55}} - \frac{R_{23}R_{34}D_{41}}{R_{33}R_{44}} - \frac{R_{23}R_{35}D_{51}}{R_{33}R_{55}}\right) - \left(\frac{R_{24}D_{41}}{R_{44}} - \frac{R_{24}R_{45}D_{51}}{R_{44}R_{55}}\right) - \frac{R_{25}D_{51}}{R_{55}}$$

$$E_{22} = D_{22} - \left(\frac{R_{23}D_{32}}{R_{33}} + \frac{R_{23}R_{34}D_{45}D_{52}}{R_{33}R_{44}R_{55}} - \frac{R_{23}R_{34}D_{42}}{R_{33}R_{44}} - \frac{R_{23}R_{35}D_{52}}{R_{33}R_{55}}\right) - \left(\frac{R_{24}D_{42}}{R_{44}} - \frac{R_{24}R_{45}D_{52}}{R_{44}R_{55}}\right) - \frac{R_{25}D_{52}}{R_{55}}$$

References

1. dos Santos, G.H.; Mendes, N. Numerical analysis of passive cooling using a porous sandy roof. *Appl. Therm. Eng.* **2013**, *51*, 25–31. [CrossRef]
2. Bennai, F.; Abahri, K.; Belarbi, R.; Tahakourt, A. Convective and conductive thermal homogenization for non-saturated porous building materials: Application on the thermal conductivity tensor. *Therm. Sci.* **2018**, *22*, 2367–2378. [CrossRef]
3. Liu, W.; Huang, X.; Riffat, S. Heat and mass transfer with phase change in a rectangular enclosure packed with unsaturated porous material. *Heat Mass Transf.* **2003**, *39*, 223–230. [CrossRef]
4. Chen, W.; Zhang, S.; Zhang, Y. Analysis on the cooling and soaking-up performance of wet porous wall for building. *Renew. Energy* **2018**, *115*, 1249–1259. [CrossRef]
5. dos Santos, G.H.; Mendes, N. Heat, air and moisture transfer through hollow porous blocks. *Int. J. Heat Mass Transf.* **2009**, *52*, 2390–2398. [CrossRef]
6. Cao, L.; Fu, Q.; Si, Y.; Ding, B.; Yu, J. Porous materials for sound absorption. *Compos. Commun.* **2018**, *10*, 25–35. [CrossRef]
7. Ning, J.; Zhao, G. Sound absorption characteristics of multilayer porous metal materials backed with an air gap. *J. Vib. Control* **2016**, *22*, 2861–2872. [CrossRef]
8. Zhu, J.; Sun, J.; Tang, H.; Wang, J.; Ao, Q.; Bao, T.; Song, W. Gradient-structural optimization of metal fiber porous materials for sound absorption. *Powder Technol.* **2016**, *301*, 1235–1241. [CrossRef]
9. Gao, N.; Luo, D.; Cheng, B.; Hou, H. Teaching-learning-based optimization of a composite metastructure in the 0–10 kHz broadband sound absorption range. *J. Acoust. Soc. Am.* **2020**, *148*, EL125–EL129. [CrossRef]
10. Gao, N.; Tang, L.; Deng, J.; Lu, K.; Hou, H.; Chen, K. Design, fabrication and sound absorption test of composite porous metamaterial with embedding I-plates into porous polyurethane sponge. *Appl. Acoust.* **2021**, *175*, 107845. [CrossRef]

11. Choy, Y.S.; Huang, L.; Wang, C. Sound propagation in and low frequency noise absorption by helium-filled porous material. *J. Acoust. Soc. Am.* **2009**, *126*, 3008–3019. [CrossRef]
12. Taghipour, A.; Dardel, M. Sound transmission loss in functionally graded porous metastructural plate with absorber. *J. Vib. Control* **2023**, *30*, 779–794. [CrossRef]
13. Yuan, W.H.; Liao, H.T.; Gao, R.X.; Li, F.L. Vibration and sound transmission loss characteristics of porous foam functionally graded sandwich panels in thermal environment. *Appl. Math. Mech.* **2023**, *44*, 897–916. [CrossRef]
14. Domenico, S.N. Effect of water saturation on seismic reflectivity of sand reservoirs encased in shale. *Geophysics* **1974**, *39*, 759–769. [CrossRef]
15. Tuncay, K.; Corapcioglu, M.Y. Wave Propagation in Poroelastic Media Saturated by Two Fluids. *J. Appl. Mech.-Trans. Asme* **1997**, *64*, 313–320. [CrossRef]
16. Lo, W.; Sposito, G.; Majer, E. Wave propagation through elastic porous media containing two immiscible fluids. *Water Resour. Res.* **2005**, *41*, 2. [CrossRef]
17. Biot, M.A. Theory of propagation of elastic waves in a fluid-saturated porous solid. I. Low-frequency range. *J. Acoust. Soc. Am.* **1956**, *28*, 168–178. [CrossRef]
18. Biot, M.A. Theory of propagation of elastic waves in a fluid-saturated porous solid. II. Higher frequency range. *J. Acoust. Soc. Am.* **1956**, *28*, 179–191. [CrossRef]
19. Biot, M.A. Mechanics of deformation and acoustic propagation in porous media. *J. Appl. Phys.* **1962**, *33*, 1482–1498. [CrossRef]
20. Garg, S.K.; Nayfeh, A.H. Compressional wave propagation in liquid and/or gas saturated elastic porous media. *J. Appl. Phys.* **1986**, *60*, 3045–3055. [CrossRef]
21. Kang, Y.; Wei, P.; Li, Y.; Zhang, P. Modeling elastic wave propagation through a partially saturated poroviscoelastic interlayer by fractional order derivatives. *Appl. Math. Model.* **2021**, *100*, 612–631. [CrossRef]
22. Berryman, J.G.; Thigpen, L.; Chin, R.C.Y. Bulk elastic wave propagation in partially saturated porous solids. *J. Acoust. Soc. Am.* **1988**, *84*, 360–373. [CrossRef]
23. Yun, Y.; Miao, G.; Zhang, P.; Huang, K.; Wei, R. Nonlinear acoustic wave propagating in one-dimensional layered system. *Phys. Lett. A* **2005**, *343*, 351–358. [CrossRef]
24. Lin, H.-J.; Wang, C.-N.; Kuo, Y.-M. Sound transmission loss across specially orthotropic laminates. *Appl. Acoust.* **2007**, *68*, 1177–1191. [CrossRef]
25. Lin, H.-J.; Wang, C.-N.; Kuo, Y.-M. Characterizing the Sound Insulation of a Specially Orthotropic Multi-Layered Medium. *J. Mech.* **2007**, *23*, 63–68. [CrossRef]
26. Shahsavari, H.; Talebitooti, R.; Kornokar, M. Analysis of wave propagation through functionally graded porous cylindrical structures considering the transfer matrix method. *Thin-Walled Struct.* **2020**, *159*, 107212. [CrossRef]
27. Castaings, M.; Hosten, B. Delta operator technique to improve the Thomson–Haskell-method stability for propagation in multilayered anisotropic absorbing plates. *J. Acoust. Soc. Am.* **1994**, *95*, 1931–1941. [CrossRef]
28. Zhang, X.; Rui, X.; Zhang, J.; Gu, J.; Zhang, L. Statics analysis based on the reduced multibody system transfer matrix method. *Multibody Syst. Dyn.* **2023**, 1–25. [CrossRef]
29. Lu, H.; Rui, X.; Zhang, X. Transfer matrix method for linear vibration analysis of flexible multibody systems. *J. Sound Vib.* **2023**, *549*, 117565. [CrossRef]
30. Khurana, P.; Boeckx, L.; Lauriks, W.; Leclaire, P.; Dazel, O.; Allard, J.F. A description of transversely isotropic sound absorbing porous materials by transfer matrices. *J. Acoust. Soc. Am.* **2009**, *125*, 915–921. [CrossRef]
31. Parrinello, A.; Ghiringhelli, G.; Atalla, N. Generalized Transfer Matrix Method for periodic planar media. *J. Sound Vib.* **2019**, *464*, 114993. [CrossRef]
32. Xue, Y. *Modelling and Design Methodologies for Sound Absorbing Porous Materials When Used Layered Vibration Dampers*; Purdue University: West Lafayette, IN, USA, 2019. [CrossRef]
33. Chen, W.; Xia, T.; Hu, W. A mixture theory analysis for the surface-wave propagation in an unsaturated porous medium. *Int. J. Solids Struct.* **2011**, *48*, 2402–2412. [CrossRef]
34. Bolton, J.; Shiau, N.-M.; Kang, Y. Sound transmission through multi-panel structures lined with elastic porous materials. *J. Sound Vib.* **1996**, *191*, 317–347. [CrossRef]

Disclaimer/Publisher's Note: The statements, opinions and data contained in all publications are solely those of the individual author(s) and contributor(s) and not of MDPI and/or the editor(s). MDPI and/or the editor(s) disclaim responsibility for any injury to people or property resulting from any ideas, methods, instructions or products referred to in the content.